Hydrol. Earth Syst. Sci. Discuss., 9, 10595–10655, 2012
www.hydrol-earth-syst-sci-discuss.net/9/10595/2012/
doi:10.5194/hessd-9-10595-2012

Hydrology and Earth System Sciences Discussions

Connected flow paths as first order control on critical zone water flows: coincidence or self-organized optimality?

E. Zehe[1], **T. Blume**[2], **A. Kleidon**[3], **U. Ehret**[1], **U. Scherer**[1], **and M. Westhoff**[1]

[1]Karlsruhe Institute of Technology (KIT), Germany
[2]GFZ German Research Centre for Geosciences, Section 5.4 Hydrology, Germany
[3]Max-Planck-Institut für Biogeochemie, Jena, Germany

Received: 15 August 2012 – Accepted: 30 August 2012 – Published: 20 September 2012

Correspondence to: E. Zehe (erwin.zehe@kit.edu)

Published by Copernicus Publications on behalf of the European Geosciences Union.

Abstract

This study proposes a theoretical framework that links hydrological dynamics to thermodynamics, with emphasis on dynamics and dissipation of free energy and production of entropy in the critical zone. Based on this theory we analyse simulations with a physically based hydrological model in the Weiherbach and the Malalcahuello catchments to learn about free energy dynamics and entropy production in these different hydro-climatic and hydro-pedological settings. Results for the Weiherbach catchment suggest the existence of a thermodynamic optimal hillslope structure as a result of co-evolution of biotic patterns and the soil catena. This optimum structure allowed acceptable un-calibrated reproduction of observed rainfall-runoff behaviour when being used in a catchment model – in fact it came close to the best fit. Results corroborate furthermore that connected network-like structures – vertical preferential pathways and the river network in this case – act as dissipative structures by accelerating flow against driving gradients, which implies accelerated entropy production. For the Malalcahuello catchment we found that maximum drainage is the functional optimum hillslope structure. This is explained by the very wet, energy limited climate, the presence of non-cohesive highly permeable ash soils and the different mechanism causing preferential flow.

1 Introduction

Hydrological research and models have traditionally been focused on predictions of water driven hazards, or the water balance. While this is a story of on-going success, we still struggle to predict how the catchment structure and distributed dynamics control integral system responses, especially at the scale of intermediate systems. According to Dooge (1986), intermediate catchments are heterogeneous systems with a strong degree of spatial organization. Their integral response is controlled by the way how organized patterns of vegetation, soil properties and preferential flow paths

HESSD
9, 10595–10655, 2012

dynamically interact with the space time patterns of boundary conditions (Schulz et al., 2006; Uhlenbrook, 2006; Zehe and Sivapalan, 2009; Phillips, 2006). All these patterns and structures – we subsume as catchment architecture – have up to now been shaped by the same flow processes they control in the present (Phillips, 2006) and can thus be regarded as their long term structural fingerprints. The key question behind this study is thus whether a better understanding of the "cause" – i.e. why organized structures in catchments have been formed and persist – might be a key for better understanding and predicting how organized structures control critical zone water flows.

1.1 Catchment organization and the search for organizing principles

A close look at catchments as hydro-geo-ecosystems reveals a highly organized architecture that is characterized by typical patterns, of topography, soil and vegetation and self-affine flow networks at all scales. Textural elements – soils and parent rock – provide a mechanical and stable matrix for growth of terrestrial biota and soil formation. They conserve storage of water and dissolved nutrients against gravity and root extraction, because water acts as wetting fluid in the pore space. The pore size distribution of a soil is at the same time a fingerprint of the work that up to now has been performed by weathering processes. As a long range and strong spatial covariance is claimed by Kondepudi and Prigogine (1998) to be generally a fingerprint of spatial organization, an apparent covariance of soil hydraulic properties is a measure of spatially organized storage within a given soil type. Spatial organization of textural elements and thus storage at the hillslope scale is reflected by the existence of a typical soil catena (Zehe and Fluhler, 2001; Zehe and Bloeschl, 2004).

Textural storage elements are interspersed with strikingly self-similar network-like structures which organize export and redistribution of water, solutes and sediments. Following Bejan (2007) we name them flow structures or flow networks. These flow structures have been created either by biota (earth worms, moles, voles, plant roots) or by dissipative processes – soil cracking (Zehe et al., 2007) or fluvial erosion – in a self-reinforcing manner (Kleidon et al., 2012; Howard, 1990). Regardless of their different

HESSD
9, 10595–10655, 2012

origin, connected flow structures exhibit similar topological characteristics and similar functioning: they are connected flow paths of very low specific flow resistances (there is no bottleneck along this flow path) and thus allow for high mass flows even at small driving potential gradients. Hence, flow structures organize and dominate drainage and redistribution at almost any scale:

- Vertical flow structures (worm burrows or soil cracks) organize and dominate vertical flows and thus redistribution of water at the plot scale – this is usually referred to as vertical preferential flow (Beven and Germann, 1982; Vogel, 2005; Klaus and Zehe, 2010, 2011);
- Surface rill and gully networks organize and dominate hillslope scale overland flow response and sediment export (Bull and Kirkby, 1997; Kirkby et al., 2003; Poesen et al., 2003; Shao et al., 2005; Parkner et al., 2007);
- Subsurface pipe networks at the bedrock interface organize hillslope scale lateral subsurface water and tracer flows (Lindenmaier et al., 2005; Weiler and McDonnell, 2007; Wienhöfer et al., 2009); this is usually referred to as lateral preferential flow in pipe systems;
- The river network directs flows of water, dissolved matter and sediments to the catchment outlet and finally across continental gradients to the sea (Rinaldo et al., 1996; Rodriguez-Iturbe and Rinaldo, 2001; Kleidon et al., 2012; Howard 1990).

All these typical patterns of textural elements, flow networks and biota co-evolved over "long" time scales (Dietrich and Perron, 2006) in response to the same dissipative processes they organize at the present time in a self-reinforcing manner. The latter must necessarily be true for allowing these structures and biota to persist. Self-reinforcement and positive feedbacks might imply that certain system architectures are "closer" to a functional optimum compared to other possible system architectures. This vague idea has inspired various scientists to suggest optimality principles to explain

HESSD
9, 10595–10655, 2012

organization of ecosystems, landscapes and flow networks. Bejan's constructural law (Bejan et al., 2008) postulates that "flow systems evolve towards an optimal structure by allowing the currents greater and greater access to the system they flow through". This is a very well-reasoned diagnostic statement, but difficult to falsify as "greater access" is somewhat imprecise. Rodriguez-Iturbe et al. (1998), Rodriguez-Iturbe and Rinaldo (2001) as well as Rinaldo et al. (1996) employed thermodynamics to explain the organization of river networks as "least energy structures", which minimize local energy dissipation at a steady state configuration. Kleidon and Schymanski (2008) proposed that most processes in the hydrological cycle, including soil wetting, are irreversible and produce entropy. The hypothesis of Maximum Entropy Production suggests that an optimal steady state system architecture is organized such that exchange fluxes of mass and energy maximise entropy production (MEP). The MEP hypothesis has been used to successfully predict states of planetary atmospheres (Lorenz et al., 2001) or to identify parameters of general circulation models (Kleidon et al., 2006). Porada et al. (2011) recently used MEP to constrain parameters for a physically based model based on multi 1-D columns to simulate the water balance of the largest 35 catchments on Earth. Zehe et al. (2010) showed within a numerical study that connected vertical macropore networks increase depletion of matric potential gradients and thus dissipation of free energy during rainfall events. They speculated that an optimal hillslope architecture maximizes reduction of free energy (MED) during rainfall events as this minimizes time to thermodynamic equilibrium. However, they did not find an apparent optimum in their study, which focused exclusively on free energy dynamics in soil. MED and MEP are in fact equivalent (see next section for a brief introduction into thermodynamics). The idea of "Maximum Power" states that an ecosystem/organism is "fittest" if it maximises power and thus extraction of free energy from persistent gradients (Odum, 1969; Lotka, 1922a, b). This implies that a maximum amount of free energy is available to be transformed into mechanical work (movement) and metabolic processes. This is deemed as an advantage against other competitors. MEP, MED and

HESSD
9, 10595–10655, 2012

Maximum Power are equivalent during steady state conditions, as will be explained in the next subsection.

1.2 Common grounds and common difficulties of organizing principles

All these different principles have the following features in common. They suggest a thermodynamic treatment of the system. This implies the existence of thermodynamic macro scales in environmental systems: because thermodynamic state variables are only well defined for a representative ensemble. In simple systems such as a gas the number of gas molecules determines whether ergodic conditions are reached and a thermodynamic treatment is justified. Identification of similar macro scales that assure ergodicity in the critical zone is however not a straight forward issue (Zehe et al., 2006; Lee et al., 2007; Reggiani et al., 1998; Bloeschl and Sivapalan, 1995).

Furthermore, these principles assume steady state conditions, with respect to (a) the catchment architecture as well as (b) water, mass and energy dynamics. While the first assumption is justified at the daily to monthly scale time (as morphological processes are slow as long as the hydro-meteorological forcing is not too extreme), the latter assumption is inadequate. Mass- or energy inputs into the catchment occur in the form of rainfall or as solar radiation. These forcing regimes are alternating and thus intermittent; we speak thus of the rainfall and the radiation driven context. Due to the intermittent nature of these forcing regimes, the time scale for defining a thermodynamic optimum should be small against the morphological time scales but large enough to include the typical variability of forcing events and flow processes.

The role of flow networks in free energy dynamics of the critical zone depends furthermore on the prevailing forcing context. During radiation driven conditions, landscape compartments deplete a vertical temperature gradient that is build up by depleting a gradient in the radiation fluxes. These temperature gradients are very steep close to the soil surface (both above and below ground) and close to the plant leaves. Evaporation is a relatively slow water mass flux, of order 0.1 mm h^{-1}, that is strongly dominated by plant transpiration. Due to the large specific heat of vaporisation this

HESSD
9, 10595–10655, 2012

processes is nevertheless very efficient at depleting these temperature gradients, thereby depleting water potential gradients in the Prandtl layer near the soil surface. Evaporation is however strongly reduced during rainfall events and evaporation fluxes are two orders of magnitude slower than rainfall intensities that can reach up to tens of $mm\,h^{-1}$. If rainfall did accumulate only at the land surface and in the top soil this would imply fast rising potential energy gradients, high mechanical loads and a reduced shear stability of the soil (Lindenmaier et al., 2005; Wienhofer et al., 2011; Hinkelmann et al., 2011; Ehlers et al., 2011). Depletion of these large gradients and mechanical stressors is only possible by means of fast mass flows that redistribute water in soil and export "excess water" from the system. We suggest that flow networks optimise free energy dynamics mainly during rainfall-driven conditions, when large mass flows are the key for efficient reduction of free energy. They are of minor importance during radiation-driven conditions, when large energy fluxes are the key for efficient dissipation/reduction of free energy.

1.3 Objectives, key assumptions and underlying hypotheses

In the present study we thus focus on connected flow structures in the critical zone and their role in dynamics of free energy and production of entropy when activated during rainfall driven conditions. Our approach is:

- to employ the physically based hydrological model CATFLOW that addresses all the relevant hydrological processes in the critical zone in a coupled way (most of the studies listed above are based on strongly simplified models);
- to use behavioural model structures: This means they have been shown to closely portray system behaviour and its architecture in a sense that they reproduce distributed observations of soil moisture and catchment scale discharge and represent the observed structural and textural signatures of soils, flow networks and vegetation;

HESSD
9, 10595–10655, 2012

– to simulate the full concert of hydrological processes at the hillslope and headwater scales for meaningful perturbations of the behavioural model structure and compare them with respect to dynamics of free energy and production of entropy.

The study areas are two very well investigated research catchments: the Weiherbach (Germany) and the Malalcahuello headwaters (Chile), which are located in distinctly different hydro-climatic, geological and land use settings.

Before providing a brief background in thermodynamics and further elaborating the necessary theory, the underlying data base and simulation results, we present the assumptions and key hypotheses underlying this study and propose several implications of these hypotheses which are falsifiable with the outlined approach. We assume that possible hydro-geo-ecosystem configurations are constrained by the climate and geological setting, available resources for biota (sunlight, phosphorus, nitrogen, water) and reflect thus on the amount of work that has been performed by past mass and energy flows and biota, given these constraints. This implies that any scenario should respect limitations in the degrees of freedom arising from these constraints.

We focus on hydrological systems whose spatial configuration is – though being far from thermodynamic equilibrium – in steady state. This implies that mass flows do not perform any work to create or destroy flow structures in the system and that the life cycles of the vegetation community are stationary. The entire available free energy that flows through the system is used to redistribute water within the system (thereby depleting gradients) and to export water against persistent gradients as well as to maintain the stationary life cycle of functional vegetation. In this case we may use equilibrium thermodynamics to analyse dynamics of free energy in the critical zone. We do not explicitly address the case of strong interactions between mass flows and structures, which means that structures are destroyed or evolve and phase transitions occur (Kleidon et al., 2012). Based on these assumptions we hypothesise that:

– H1: macroscopically connected flow networks enhance redistribution of mass against macroscale gradients and thus dissipation and export of free energy, because they minimize local free energy dissipation per unit mass flow continuously

HESSD
9, 10595–10655, 2012

along the flow path (Kleidon et al., 2012). This implies (I1) mechanical stability of the flow network and of the textural storage elements and thus of the entire system against frequent disturbances under stationary conditions.

– H2: a steady state architecture of a hydro-geo-ecosystem is closer to a functional optimum than other possible configurations if it dissipates and exports more of the available free energy by redistributing mass and energy within and exporting mass and energy from the system (in the following we will use the term dissipation of free energy to subsume all processes that reduce free energy of the system). This implies (I2) that the system approaches a dynamic equilibrium state characterised by a minimum in free energy faster than other configurations and that less free energy from flow against persistent gradients is available to perform work on the system architecture itself. This is deemed to be favourable for mechanical stability of the system.

These hypotheses imply furthermore that:

– I3: recent terrestrial geo-ecosystems – at least those that have been strongly modified by fluvial erosion, soil formation and biotic activities – should at a discrete hierarchy of thermodynamic macroscales be very efficient in dissipating and exporting free energy and close to a functional optimum (when existent);

– I4: in the long term the optimally structured system would serve the "act" of depleting the macro scale gradients in a minimum time by maximising mass flows against them (if these gradients were not sustained by external processes).

The remaining study is structured as follows. In Sect. 2 we briefly introduce the thermodynamic background, suggest a hierarchy of hydrological and thermodynamic macro scales where H1 and H2 should apply, and develop the necessary theory to link physically based hydrology and thermodynamics. Section 3 introduces the two study areas, the Weiherbach and the Malalcahuello catchments, and provides a brief description of the numerical model. It then explains the numerical experiments that were performed

HESSD
9, 10595–10655, 2012

to shed light on free energy dynamics and entropy production to test H1, H2 and the implications I1, I2 and I3 at the hillslope and headwater scales. This is followed by presentation and interpretation of the modelling results in Sect. 4 and discussion and conclusions in Sect. 5.

2 Theory

2.1 Thermodynamic background

Thermodynamics is a fundamental theory of physics that deals with the general rules and limits for transforming energy of different types. It is commonly applied to conversions that involve heat, and to systems with fixed boundary conditions, such as a heat engine. The scope of thermodynamics is, however, much wider, as will be shown in Sect. 2.3. The first law of thermodynamics is a more precise formulation of the law of energy conservation and states that the change of total internal energy of a thermodynamic system is equal to the change in heat dQ plus the change in free energy dF (see Sect. 2.3 for definition of free energy in the critical zone).

$$\mathrm{d}U = \mathrm{d}Q + \mathrm{d}F \tag{1}$$

Any exchange of heat is proportional to the change in entropy dS times the absolute temperature T. Hence

$$\mathrm{d}S = \frac{\mathrm{d}Q}{T} \tag{2}$$

From Eq. (2) it becomes evident that exchange of heat dQ against a temperature gradient is associated with the net production of entropy while the temperature, gradient is depleted: the cooler reservoir gains $\mathrm{d}S = \mathrm{d}Q/T_{\mathrm{low}}$ and the warmer reservoir loses $-\mathrm{d}S = -\mathrm{d}Q/T_{\mathrm{high}}$. The second law of thermodynamics states that entropy cannot be

HESSD
9, 10595–10655, 2012

consumed but stays constant during reversible processes and is produced during irreversible mixing processes. Depletion of temperature gradients, or more generally depletion of any gradient, is thus associated with production of entropy, irreversibility and a reduction in free energy, while total energy is conserved. For isolated systems this implies that the system evolves to a state of maximum entropy, which implies perfect mixing, absence of any gradient and thus maximum disorder. Open systems may, however, exchange energy and mass with their environment. Organized structures may hence form and persist, as long as incoming fluxes provide the necessary free energy to form and later on maintain these structures and to export entropy that is produced during related irreversible processes across the systems boundary to the environment. The entropy balance equation of an open system is thus the sum of the entropy produced by irreversible processes, σ, and the net entropy exchange with the environment NEE.

$$\frac{\mathrm{d}S}{\mathrm{d}t} = \sigma + \mathrm{NEE} \tag{3}$$

Persistent energy and mass flows through the system require, however, persistent driving macroscale gradients that span across the entire system: the Bernard cell and Planet Earth are prominent examples. Heat fluxes along these macroscale temperature gradients would deplete them, if there were no external processes that worked against its depletion. For the Bernard cell this is the heating at the bottom and cooling at the top of the cell; for Planet Earth this is planetary radiation exchange (the poles receive less radiation input than the equator).

2.1.1 Maximum Entropy Production and related principles

The MEP principle states that an open system is in steady state structured in such a way that entropy production is maximized. A term for entropy production may be derived from the work balance of an open system, which can be written as the sum of generated power P minus the amount of dissipation of free energy into heat by

HESSD
9, 10595–10655, 2012

production of entropy due to irreversible processes:

$$\frac{dF}{dt} = P - T\sigma = m\boldsymbol{v} \cdot \boldsymbol{\nabla}\Phi - T\sigma. \quad (4)$$

Note that mechanical Power is force F times velocity $\boldsymbol{v}$. As force is mass times acceleration, and acceleration is in conservative force fields equal to a potential gradient $\boldsymbol{\nabla}\Phi$, power is mass flow times the driving potential gradient (In case of electrical power we have current i.e. charge flow times the electric tension, which is the gradient in electric potential). In steady state, when dF/dt is equal to zero, production of entropy is thus equal to flow times the driving gradient divided by the absolute temperature. Maximization of entropy production in steady states implies thus maximization of flow against the macroscale gradient, maximization of power in this flow and maximum reduction of free energy of the system (compare Eq. 1). In the case where there were no external processes that sustained the gradients this would imply that the system reached thermodynamic equilibrium through depletion of the driving macro scale gradient as fast as possible. The external processes that sustain potential gradients at the land surface/critical zone are re-distribution of water by means of rainfall as a fast process and iso-static uplift as a very slow process (Kleidon et al., 2012).

2.2 System boundaries, controls on flows and thermodynamic macro scales

2.2.1 Upper and lower boundaries

The very first step to treat the critical zone in thermodynamic terms is to define the system's boundary. The critical zone extends from the land surface and the surface of the vegetation (upper boundary), through the unsaturated soil zone down to the groundwater surface, which forms the lower boundary. The definition of lateral system boundaries is a little more involved as they separate the different scale levels for which a thermodynamic treatment of critical zone water dynamics is deemed as justified. Analogous to the gas example we need ergodic conditions but here with respect to the

HESSD
9, 10595–10655, 2012

potential gradients and the resistances that control water, heat and mass fluxes within the critical zone and across its boundaries. This means the system must be much larger than the critical length scales of the landscape elements that control potential gradients and resistances.

2.2.2 Gradients and resistances controlling mass flows in the landscape

Fast lateral flows are driven by gradients in piezometric heads and thus potential energy. These potential gradients arise at inclined material interfaces, i.e. the land surface, the bedrock surface and the groundwater surface. They range from zero to the hydrostatic geo-potential gradient. Except for groundwater dominated systems these potential gradients are thus largely determined by the quasi static micro and macro topography of these interfaces. Vertical subsurface water fluxes in soil are driven by vertical gradients in soil hydraulic potential (matric potential plus gravity potential); soil texture and the water retention curve of a soil ($\psi(\theta)$) act as time invariant controls; soil moisture and depth to groundwater act as time variant controls of these potentials (see Fig. 1). Matric potential gradients in fine textured soils can be much steeper than geo potential gradients and range up to values of $100\,\mathrm{m\,m^{-1}}$, especially during dry spells.

Gradients in plant and atmospheric water potential are controlled by plant physiology and air humidity and air temperature. These are in fact the steepest gradients that drive fluxes (Porada et al., 2011). Canopy resistance depends on the stomatal resistance and the Leaf Area Index. Stomatal resistance is deemed to depend on PAR (photosynthetic active radiation), water availability in the root zone and the physiology of the plant of interest.

Subsurface flow resistance R is a property of the control volume (not just a material property), depending on texture i.e. soil hydraulic conductivity $1/k(\theta)$ and its characteristic lengths. In general, flow resistance is a tensor and can be strongly anisotropic. Apparent flow networks (pipes, macropores) connected in the direction of the driving potential gradients $\nabla\Phi$ reduce control volume resistances and result in accelerated fluxes and stronger power production/entropy production. Surface flow resistances for

HESSD
9, 10595–10655, 2012

lateral water flows depend on surface roughness and thus vegetation. Again, apparent connected networks of rills in the direction of the driving gradient $\nabla\Phi$ reduce control volume resistances and result in accelerated overland flow and shorter response times of hillslopes. Common characteristic of connected flow networks is, thus, that they reduce control volume resistance by means of a spatially organized arrangement of materials; this implies strong anisotropy in control volume resistance along different possible flow directions. Note that this internal organization due to apparent flow structures must not imply any change in geo statistical properties (mean, variance, covariance).

2.2.3 Lateral boundaries rendering scale levels

We can now define precisely the criteria needed for the definition of lateral system boundaries, with which to allow a meaningful thermodynamic treatment, by criteria that characterise the statistical homogeneity of driving gradients, control volume resistances and the boundary conditions:

- The system extends to next relevant minimum in (geo) potential that controls lateral mass flows. This implies the system spans the macroscale gradients that drive vertical and lateral water fluxes. Please note that the gradient is determined by strength and direction, thus significant changes with respect to average strength, actual profile/shape in vertical or lateral directions, or in average direction determine lateral boundaries of macro scales.
- The system is large enough to ensure ergodic conditions with respect to (a) variability and covariance of functional vegetation communities and soil textural elements as well as (b) the density and topology of vertical and/or lateral flow networks. This implies that the system is representative with respect to the control volume resistance along the entire extent of the driving gradients.

HESSD
9, 10595–10655, 2012

– The system is large enough to integrate the relevant spatial variability of the climatic forcing or small enough to neglect this spatial variability. This implies homogeneity with respect to the regimes of mass and energy inputs.

These criteria are suitable to define the same hierarchy of macroscales – plot, hillslope, headwater and river basin – that have been used intuitively in hydrology for a long time (Fig. 2). The plot scale is characterised by the absence of lateral geo-potential gradients. Its lateral extent depends (a) on the length up to which lateral gradients in matric potentials can be neglected and a laterally uniform potential can be defined, (b) on lateral correlation lengths of soil matrix properties as well as the length scale at which the average density of vertical preferential pathways changes to ensure ergodic conditions.

The hillslope scale extends from the watershed boundary (this is in fact where driving lateral geo potential gradients flip their direction and point into different catchments) down to the next local minimum in geo-potential, which is the riparian zone. Note that only "macroscopically" connected flow networks that extend continuously to a system boundary (either the surface or the riparian zone) play a pivotal role in organizing mass flows and dissipation of free energy, because other networks do not allow for fast flows against the entire extent of the vertical and lateral driving gradient.

The next scale level is the headwater scale, where several hillslopes are interconnected by a river net that routs water, sediment and nutrients in an organized manner downstream. Flow accumulation of hillslopes in headwaters is however still strongly confluent. Transitions to higher scale levels (catchment and river basin) might be defined based on significant changes in network topology (Strahler order), related changes in flow accumulation (to parallel and even divergent hillslopes), as well as on changes in climate, landuse and textural elements (geological strata, change in soil landscape).

HESSD
9, 10595–10655, 2012

2.3 Free energy dynamics due to fast and slow dynamics in the critical zone

Dynamics of free energy in the critical zone are compiled by various forms of free energy exchange as follows:

$$\underset{\text{I}}{\mathrm{d}F} = \underset{\text{I}}{-\mathrm{d}(\mathrm{ST})} \underset{\text{II}}{-\mathrm{d}(pV)} \underset{\text{III}}{+d(\sum_i \mu_i M_i)} \underset{\text{IV}}{+\mathrm{d}(\sum_j \Phi_j M_i)} \underset{\text{V}}{+\mathrm{d}(\boldsymbol{v}\cdot\boldsymbol{p})} \underset{\text{VI}}{+\mathrm{d}(\sigma_w A_\mathrm{w})}... \quad (5)$$

Free energy is minimal during thermodynamic equilibrium and each form of free energy is defined as a product of conjugated pairs of an intensive and extensive state variable of the critical zone. The first term relates changes in entropy S (J/K) and in absolute temperature T (K) and describes the change in free energy due to heating/cooling or to irreversible processes such as evaporation. The second term refers to changes in mechanical pressure p ($\mathrm{N\,m^{-2}}$) and volume V ($\mathrm{m^3}$) and describes the change in free energy due to mechanical work, for instance due to shrinking/ swelling soils or due to a slowly increasing mechanical load on the system (for instance by increasing biomass). The third term refers to changes in chemical potential μ ($\mathrm{m^2\,s^{-2}}$) and mass M (kg) of the constituent i and characterizes the change in free energy due to chemical mixing and reactions. The fourth term refers to changes in geo potential Φ ($\mathrm{m^2\,s^{-2}}$) and the mass M in the gravity field and characterizes the change in free energy due to fast but also slow mass flows in the geo potential field. In the short term this is also largely affected by soil water dynamics and surface runoff, as further elaborated below. The fifth term refers to changes in velocity of mass flows $\boldsymbol{v}$ ($\mathrm{m\,s^{-1}}$) and the momentum $\boldsymbol{p}$ ($\mathrm{kg\,m\,s^{-1}}$) and thus describes changes in free energy due to changes in kinetic energy of mass flows. This is largely related to transient and steady state discharge in the catchments, as further elaborated below. The last term describes changes in free energy due to a change in surface tension of water σ_w ($\mathrm{kg\,s^{-2}}$) and the water-air interface A_w ($\mathrm{m^2}$) in the pore space of the soil.

The next important step is to separate soil water mass from other masses. Total stored water mass in the pore space and geo potential of water in the subsurface are

HESSD
9, 10595–10655, 2012

directly related to soil water content θ ($m^3\,m^{-3}$) and the height z above the groundwater surface:

$$M = \rho \iiint \theta \mathrm{d}V$$
$$\Phi = gz \tag{6}$$

Where g is the acceleration of the earth ($9.81\,m\,s^{-2}$), ρ is the density of water ($kg\,m^{-3}$) and z is elevation above the ground water surface (M). Inserting of Eq. (6) into term four of Eq. (5) allows separation of soil water mass from the other masses and leads to:

$$\mathrm{d}F = -\mathrm{d}(\mathrm{ST}) - \mathrm{d}(pV) + \mathrm{d}(\sum_i \mu_i M_i) + \mathrm{d}(\sum_i \Phi_i M_i) + \mathrm{d}(gz\rho V\theta) + \mathrm{d}(\boldsymbol{v}\cdot\boldsymbol{p}) + \mathrm{d}(\sigma_w A_w) \tag{7}$$

Note that the index i in term four refers to surface water and sediment mass.

Next we establish a link for the last term in Eq. (7) to the definition of matric potential/capillary potential of water in soil. Surface tension of water and capillary potential are linked through the curvature radius r of the air-water interface.

$$\psi(\theta) = \frac{2\sigma_w}{\rho g r} \Leftrightarrow \sigma_w = \frac{1}{2}\rho g \psi(\theta) r$$
$$\frac{1}{2}A_w r \approx V_w = \theta V \tag{8}$$

Furthermore we approximate 1/2 $A_w r$ as the volume of the water phase V_w. This is equal to soil moisture times the total volume of the soil. Insertion of Eq. (8) into the last term of Eq. (7) and rearrangement of terms yields:

$$\mathrm{d}F = -\mathrm{d}(\mathrm{ST}) - \mathrm{d}(pV) + \mathrm{d}(\sum_i \mu_i M_i) + \mathrm{d}(\sum_i \Phi_i M_i) + \mathrm{d}(\rho g \psi(\theta) V\theta) + \mathrm{d}(\rho g z V\theta) + \mathrm{d}(\boldsymbol{v}\cdot\boldsymbol{p}) \tag{9}$$

Applying Leibnitz rule and rearranging terms with respect to dominant processes, their characteristic time scales and governing equations (if known) yields the following ten

HESSD
9, 10595–10655, 2012

terms:

$$
\begin{aligned}
&\mathrm{d}F = -S\mathrm{d}T - T\mathrm{d}S \xrightarrow{\text{Term 1}} \text{Heat balance eq., Entropy balance eq.}\\
&-p\mathrm{d}V \xrightarrow{\text{Term 2}} \text{Soil shrinking/swelling}\\
&+\rho g V \psi(\theta)\mathrm{d}\theta + \rho g V z \mathrm{d}\theta \xrightarrow{\text{Term 3}} \text{Soil water dynamics, Richards eq.}\\
&+2M\boldsymbol{v}\,\mathrm{d}\boldsymbol{v} + v^2\mathrm{d}M \xrightarrow{\text{Term 4}} \text{Runoff, Saint–Venant \& Mass balance eq.}\\
&+\sum_i \mu_i \mathrm{d}M_i + \sum_i M_i \mathrm{d}\mu_i \xrightarrow{\text{Term 5}} \text{Reactive transport, Conv.–Disp. eq.}\\
&+\sum_i \varphi_i \mathrm{d}M_i \xrightarrow{\text{Term 6}} \text{Overland flow \& Erosion, Navier–Stokes \& Sediment balance eq.}\\
&+\rho g V \theta\, \mathrm{d}z \xrightarrow{\text{Term 7}} \text{GW–level dynamics, Darcy eq., Bousinesque eq.}\\
&-V\mathrm{d}p \xrightarrow{\text{Term 8}} \text{Growth of interannual plants, saturated soil loads}\\
&+\rho g V \theta\, \mathrm{d}\psi(\theta) \xrightarrow{\text{Term 9}} \text{Change in pore size distrubtion, soil weathering}\\
&+\left(\sum_i M_i\right)\mathrm{d}\varphi \xrightarrow{\text{Term 10}} \text{Iso–static uplift}
\end{aligned}
\tag{10}
$$

Free energy dynamics according to term 1 is determined by the heat balance and the entropy balance equations (Eq. 3) of the critical zone. This term is dominant during radiation-driven conditions, with especially the phase transition from liquid water

HESSD
9, 10595–10655, 2012

to water vapor during the evaporation process related to the term $T\mathrm{d}S$ (Kleidon and Schymanski, 2008). This term creates feedbacks on Term 3.

Term 2 is (a) related to short term cracking and swelling of the soil and is of relevance for soils containing Smectite clay minerals and (b) to long term root growth, which feeds back on Term 8.

Term 3 accounts for changes in free energy due to soil water dynamics and is thus determined by the Richards equation. Please note that during steady state, i.e. $\mathrm{d}F = 0$ and when neglecting all terms except Term 3, thermodynamic equilibrium is equal to the well-known hydraulic equilibrium of the soil.

The first part of Term 4 is only non-zero during transient flow conditions and is determined by Navier-Stokes /Saint-Venant equations. The second part in Term 4 is also non-zero during steady flow conditions and is dominated by discharge in the river net as it scales with v^2 (note flow velocities in the subsurface are 4–5 orders of magnitude smaller than in river networks and at the surface).

Term 5 accounts for reactive transport and mixing of dissolved substances in the water phase and can be characterised by coupling the Convection-Dispersion equation with Richards equation and Saint-Venant equation.

Term 6 is determined by overland flow and sediment transport, and can be quantified by coupling Saint-Venant Equation with the sediment balance. This term creates long term feedbacks on Term 10.

Term 7 accounts for a change in free energy of the critical zone due to slow changing groundwater levels, as the latter determines the level of zero geo potential in soil.

Term 8 accounts partly for even slower processes like slowly increasing mechanical pressures due to growth of inter-annual plants, for instance trees, and for mechanical loads from rainfall.

Term 9 addresses a change in matric potential at constant soil water content. This term can thus account for hysteresis or for changes in the soil water retention curve/pore size distribution, either on the short term due to soil compaction or in the long term due to soil weathering.

HESSD
9, 10595–10655, 2012

Term 10 accounts for slow changes in the geo-potential due to erosion and iso-static uplift (Kleidon et al., 2012).

As we are focusing on the steady state architectures of the critical zone as well as on free energy dynamics related to mass flows during rainfall driven conditions, we neglect Terms 1, 8, 9 and 10. Furthermore, we also neglect Term 2 as the soils in the two study areas are non-swelling and Term 4 which describes the export of kinetic energy. The latter is justified since the maximum amount of kinetic energy export by overland flow is determined by its potential energy in Term 6. Finally, we neglect Term 7 which is related to fluctuations in the groundwater surface Thus, free energy dynamics is characterized by

$$\mathrm{d}F = \rho g V(\psi(\theta) + z)\mathrm{d}\theta - \Phi \mathrm{d}M. \quad (11)$$

M summarizes all water flows that leave the system against geo potential gradients (we neglect erosion here). We may substitute Φ by gz, times sine of the slope when looking at overland flow and subsurface storm flow, and dM by the product of water density times the accumulated flow $Q\mathrm{d}t$. Finally we end up with

$$\mathrm{d}F = \rho g V(\psi(\theta) + z)\mathrm{d}\theta - gz\rho Q\mathrm{d}t. \quad (12)$$

Q summarizes all water flows that leave the system: surface runoff, groundwater recharge and subsurface storm flow at the hillslope scale or total discharge at scales larger than the headwaters. We can thus quantify free energy dynamics within the critical zone as a function of incoming and outgoing mass flows and redistribution of water within soil by solving Richards equation and simulating total overland low, interflow and groundwater recharge for a given catchment. Note there is, depending on retention properties of prevailing soils and apparent connected flow networks, a trade-off between maximizing storage and thus minimizing matric potentials of water in soil and maximising drainage and thus minimizing potential energy and enhancing the export of kinetic energy due to runoff. We will explore this trade-off for the two research areas – the Weiherbach (Germany) and the Malalcahuello headwater (Chile) – using

HESSD
9, 10595–10655, 2012

model structures that have been shown to closely portray systems behavior at the plot, hillslope and headwater scales.

3 Material and methods

3.1 Study areas and data base

3.1.1 The Weiherbach catchment

The Weiherbach catchment (South West Germany, 6.8 km^2) has been intensely monitored since 1989: this included (a) a soil and plant survey, derivation of typical soil hydraulic properties based on more than 200 soil cores (Table 1), and growth curves for arable crops, (b) monitoring of rainfall and runoff at six rain and two river gauges, (c) observation of standard meteorological variables and ET from eddy correlation data. A soil map was compiled from texture information that was available on a regular grid of 50 m spacing.

Geologically the Weiherbach valley consists of Keuper and Loess layers of up to 15 m thickness. The climate is semi humid with an average annual precipitation of 750–800 mm yr^{-1}, average annual runoff of 150 mm yr^{-1}, and annual potential evapotranspiration of 775 mm yr^{-1}. More than 95 % of the total catchment area is used for cultivation of agricultural crops or pasture, 4 % is forested and 1 % is paved area. The geomorphology is characterized by gentle slopes with a typical loess soil catena formed by erosion: moist but drained Colluvisols at the foot of the hillslopes and valley floors as well as drier Calcaric Regosols in the upper hillslope sectors. The macropore system was mapped at 15 sites by counting anecic earthworm burrows (*Lumbricus terrestris* and *Aporectodea longa)* and measuring their depth (Zehe and Flühler, 2001b; Zehe et al., 2001). This revealed a higher spatial density of larger and deeper worm burrows within the downslope Colluvisols. One likely reason for this spatial organization is that

HESSD
9, 10595–10655, 2012

earthworms find better habitat conditions due to the more even moisture regime and the higher amount of soil organic material within the Colluvisols.

These typical organized patterns of soils and macroporosity have caused a spatially organized pattern of infiltration at the slope scale (Fig. 3a, Zehe and Fluehler, 2001b) which in turn has been shown to exert a key influence on the catchment scale runoff response to extreme rainfall events (Zehe et al., 2005). Due to the absence of lateral subsurface strata, Hortonian overland flow dominates event runoff generation. Because the apparent macropores elevate infiltrability of soils, rainfall runoff events are rare. Event runoff coefficients range from 12 % during extreme thunder storms down to 2.0 %. Base flow is almost constant throughout the year. In the present study we focus on the 3.5 km^2 large upper catchment area upstream of the gauge Menzingen.

3.1.2 The Malalcahuello catchment

The Malalcahuello catchment is located on the southern slope of Volcano Lonquimay within the Reserva Forestal Malalcahuello (Fig. 3b) in the Chilean Andes. The catchment has a size of 6.26 km^2, ranges in elevation from 1120 to 1856 m with mean slopes of 51 % (27°). 80 % of the catchment is covered with native forest of the types *Araucaria* and *Nothofagus* with a dense understorey of bamboo (*Chusquea culeou*). The climate is temperate-humid with yearly rainfall ranging from 2000 to 3000 mm yr^{-1}. The soils are young, little developed volcanic ash soils with high porosities (60–80 %) and saturated hydraulic conductivity (10^{-5}–10^{-3} m s^{-1}).

Within an extensive field campaign, Blume et al. (2007, 2008a, b) instrumented a transect in a focus area with soil moisture probes, shallow piezometers, throughfall collectors and installed several rain and stream gauges in the catchment. These instruments yielded continuous data for the period 2004 to 2006. These observations of states and fluxes were complemented by auger- and electric resistivity tomography (ERT) profiles to explore strata and depth to bedrock, derivation of soil hydraulic parameters, observations of stable isotopes, river chemistry, distributed dye tracer profiles and much more. Existing data prior to this study included data from two nearby climate

HESSD
9, 10595–10655, 2012

stations where data have been measured (a) on a daily basis since 1989 and (b) on an hourly basis since 1999. A stream gauging station (maintained by the Universidad Austral) at the main outlet of the catchment has been in intermittent operation since 1998.

Note that runoff production within the Malalcahuello catchment is totally different from that in the Weiherbach. Annual runoff coefficients are of order of 60 % and thus three times larger than in the Weiherbach, while event runoff coefficients are within 4 to 19 % similar as in the Weiherbach. Overland flow is of negligible importance for runoff generation. Subsurface storm flow and mobilization of pre-event water from the riparian zone or the lower hillslope sector are the dominant lateral runoff processes (Blume et al., 2008b). The vertical trigger is fast finger flow that is caused by fairly strong hydrophobicity of these soils during the summer (Blume et al., 2009).

3.2 Model and basic model setups

3.2.1 Process components of the numerical model

The numerical experiments were conducted with the physically based model CATFLOW (Zehe et al., 2001). CATFLOW represents a hillslope along the steepest descent line as a 2-dimensional cross section that is discretized by 2-dimensional curvilinear orthogonal coordinates. The hillslope is thus assumed to be uniformly perpendicular to the slope line. Soil water dynamics are described by the Richards equation in the potential form that is numerically solved by an implicit mass conservative Picard iteration (Celia and Bouloutas, 1990). Soil hydraulic functions are described after van Genuchten (1980) and Mualem (1976). The model allows for simulation of solute transport by means of the 2-dimensional convection dispersion equation, which is solved using a particle tracking approach. Evapo-transpiration is represented by an advanced SVAT approach based on the Penman-Monteith equation, which accounts for growth of agricultural crops and annual cycles of LAI and ground cover of perennial plants. Surface runoff routing down the hillslopes and flood routing in the river net is simulated

HESSD
9, 10595–10655, 2012

based on the diffusion wave approximation of the 1-dimensional Saint-Venant equations. The latter is numerically solved by an explicit upstream finite difference scheme.

CATLFOW allows for representation of vertical and lateral preferential pathways along two main avenues. One is explicit representation as connected flow paths of low flow resistance and low retention properties. This approach was shown to be suitable to predict preferential flow and tracer transport that has been observed at the field scale (Klaus and Zehe, 2010, 2011). It was furthermore used when investigating the effect of connected flow paths on dissipation of free energy at the plot and the small field scale (Zehe et al., 2010). In the present study we will reanalyse one of the numerical experiments of Zehe et al. (2010) as explained below. The main advantage of this approach to representing preferential pathways is that it can be parameterized based on observable quantities (worm burrow density, lengths and maximum water flow rates in worm burrows). Due to its computational expense, this approach is restricted to small spatial scales and short time scales.

In the present study we use the effective approach that enlarges hydraulic conductivity by the macroporosity factor f_m when soil water saturation S exceeds a threshold S_0. Bulk hydraulic conductivity k^B is then increased linearly with relative saturation, as follows:

$$\begin{aligned} k^B &= k_s + k_s f_m \frac{S - S_0}{1 - S_0} \quad \text{if } S \geq S_0 \\ k^B &= k_s \text{ otherwise} \\ S &= \frac{\theta - \theta_r}{\theta_s - \theta_r} \end{aligned} \quad . \tag{13}$$

Where k_s is the saturated hydraulic conductivity of the soil matrix ($m\,s^{-1}$), the terms θ_s and θ_r are saturated and residual soil moisture, respectively. The macroporosity factor, f_m, is the water flow in all macropores, Q_m ($m^3\,s^{-1}$), in a water saturated model element of area A divided by the saturated water flow rate in the soil matrix. It is an effective soil property representation of how all activated macropores enhance infiltrability compared to the surrounding matrix flow.

HESSD
9, 10595–10655, 2012

This simple approach was proven to yield good predictions at different scales. Plot scale bromide transport at three sites of different macroporosity was simulated in good accordance with experimental findings (Zehe and Blöschl, 2004). In this case f_m-values were calculated from plot scale observations of worm burrow density, lengths and maximum water flow rates in worm burrows. Feasibility has been corroborated by successful simulations of tracer transport and the water balance of a complete hillslope for a period of two years (Zehe et al., 2001). Furthermore, the model performed well in a continuous simulation of the water balance of the Weiherbach catchment over a period of 1.5 yr (Zehe et al., 2001), after f_m was tuned to match the largest observed runoff event in June 1994. This approach also allowed good predictions to be made of rainfall runoff in the Malalcahuello catchment during snow free periods (Blume, 2008).

The range of f_m depends on the fact whether preferential pathways end in the soil matrix (as in the Weiherbach), which implies that hydraulic conductivity in the soil matrix controls flow in water-saturated macropores. In this case f_m ranges from 1–4, because infiltration into a given area is moderately accelerated as the macropores offer an additional amount of interface area. However, flow velocities across this additional interface still correspond to matrix flow (Beven and Clarke, 1986). When vertical and lateral preferential pathways are interconnected and extend to the stream, as in the Malalcahuello catchments, f_m values might be tuned up to values of 50–100, to reproduce or match observed fast flow reactions (Blume 2008).

3.2.2 Basic model setup for the Weiherbach catchment

For the simulation in the Weiherbach catchment we used the basic setup introduced in Zehe et al. (2001). The catchment was subdivided into 169 hillslopes and an associated drainage channel network. The hillslope model elements, typically, are 5–20 m wide, 10 m long, and the depth of each layer varies from 5 cm of the surface elements to 25 cm of the lower layers. The total soil depth represented by the model was 2 m. The Manning roughness coefficients for the hillslopes and the channels were taken from a number of irrigation experiments performed in the catchment, as well as from

HESSD
9, 10595–10655, 2012

the literature (Scherer et al., 2012). For the hillslopes the following boundary conditions were chosen: free drainage at the bottom, mixed boundary conditions at the interface to the stream, atmospheric boundary conditions at the upper boundary, no flux boundary at the watershed boundary.

Because of the spatially organized hillslope soil catena, all hillslopes in the model catchment were given the same relative catena, with Calcaric Regosol in the upper 80 % and Colluvisol in the lower 20 % of the hill. The corresponding van Genuchten-Mualem parameters are listed in Table 1. Vegetation was parameterized based on available crop patterns in the simulation period (April 1994 to September 1995) and tabulated data with typical annual cycles for LAI, plant height root depth and values for stomata resistances. Observations of macroporosity at 15 sites in the Weiherbach suggested a downslope increasing density of worm burrows. On the foot of the hillslopes the macropore volumes typically were $1.5 \times 10^{-3}\,m^3$ for $1\,m^2$ sampling area while on the top they typically were $0.6 \times 10^{-3}\,m^3$ (Zehe, 1999, his Fig. 4.1). The most parsimonious approach to represent this spatial organization is a deterministic pattern of the macroporosity factor with fixed scaled values of the macroporosity factor at each hillslope. We chose the macroporosity factor to $0.6 \times f_m$ at the upper 70 % of the hillslope, $1.1 \times f_m$ at the mid-sector ranging from 70 to 85 % of the hillslope, and $1.5 \times f_m$ at the lowest 85 to 100 % of the slope length, where f_m is a remaining free parameter. The depth of the macroporous layer was assumed to be constant throughout the whole catchment and was set to 0.5 m. As the number of macropores connected to the soil surface varies throughout the year, the f_m value was calibrated to match the hydrograph of the largest observed flood event in June 1994: 1.5 allowed the best fit (Zehe et al., 2001). This value allowed, without change, an acceptable reproduction of the discharge for a continuous simulation of 1.5 yr with a Nash-Sutcliffe coefficient of 0.8, soil moisture dynamics observed at 61 TDR stations (R^2 between 0.5 and 0.7), and of evaporation observed at the central meteorological station ($R^2 = 0.9$).

HESSD
9, 10595–10655, 2012

3.2.3 Basic model setup for the Malalcahuello catchment

For the simulation of the Malalcahuello Catchment the monitored hillslope near the catchment outlet was considered typical for the entire catchment. Due to the very fast travel times within the stream network (event response times as low as 30 min have been observed at the catchment outlet), it seemed feasible to neglect transport times within the stream. The model therefore consisted of only one hillslope of 80 m length and a total elevation difference of 60 m. Specific hillslope outflow was compared to catchment specific discharge for validation purposes. The hillslope domain had a depth of 10 m (Fig. 4). The soil layers were parameterized according to field observations and consisted of a 5 cm humus layer followed by several layers of volcanic ash soil. At 2 m depth a layer of gravel-size volcanic material is likely to function as a poorly ermeable barrier. This was represented as layer of lower permeability (compare Table 2). The lower boundary condition is modelled as a no flow boundary at the lowest 15 % of the hillslope, the rest was free drainage. The right boundary is no flow in the lower part (up to 2.5 m below ground) producing a saturated wedge in the lower part of the hillslope, above which a seepage boundary allows for hillslope outflow. Vertical and lateral hydraulic conductivity in the upper 80 cm was enlarged by a macroporosity factor. Best fit with a Nash 0.7 was achieved with a value of 50 and threshold saturation of $S_0 = 0.4$. The modelled vegetation was deciduous forest with parameter values either observed in the field or taken from the literature.

3.3 Numerical experiments

3.3.1 Experiment 1: connected flow networks as accelerators for entropy production in the Weiherbach?

The first numerical experiment was designed to test hypothesis H1 which states that connected flow structures – in our case the river network itself – enhance flows against macroscale driving gradients and thus production of entropy. The idea was to compare

HESSD
9, 10595–10655, 2012

overland flow production from headwaters with linear and nonlinear but homogeneous topography and no river net to the overland flow production of the headwater with the fully developed geomorphology: with locally inclined hillslopes and a river net. The first two setups represent possible initial configurations before fluvial structure formation has started (see Kleidon et al., 2012); the latter represents the steady state of a mature landscape (Fig. 4c).

We thus compared three different cases;

- Case 1: the basic model setup, with the f_m value that allowed the best prediction of the long term rainfall runoff behavior and water balance for a period of 1.5 yr (Fig. 4a).
- Case 2: a "catchment" size hillslope with uniform slope, with the same area, same length and the same elevation difference along its extent as the real catchment. We assigned the same effective catena and macroporosity pattern and same f_m value as in the real catchment (case 1). The crop pattern of the real catchment was assigned to this uniform hillslope by using their areal fractions. Please note that runoff that leaves the hillslope has flowed along the same catena. However, this is simulated as sheet flow and not as flow in a connected river network that interlinks 169 hillslopes, and which has cut itself into the landscape by backward erosion, as explained in Kleidon et al. (2012).
- Case 3: is identical to case 2, except that we did not assume a homogenous topography but used the hypsometric curve of the Weiherbach catchment: (areal fraction of pixels about a relative height h/H; where h is the height above the outlet and H the total elevation difference). We considered this as a representative mean hillslope form that reflects the average geomorphic shape of the hillslopes (including the presence of a riparian zone) and thus "the age" of the catchment (Fig. 4b). Again runoff flows along the same catena and is driven by the areal average of the same local geo potential gradient.

HESSD
9, 10595–10655, 2012

Simulation started at 21 April 1994 and lasted until 15 September 1995, because this is the only period where rainfall runoff events with runoff coefficients larger than 2 % occurred. Each model structure was dynamically initialized by using the final state of a two year simulation period (21 April 1992–20 April 1994), which started with hydraulic equilibrium in soil and was driven using observed boundary conditions. Flow across the lower boundary of the hillslopes was treated as groundwater recharge. In case 1 this was set as equal to the base flow contribution of the individual hillslopes and added to river flow. In the other two cases it was regarded as groundwater runoff. For each of these cases we calculated generated power from runoff as flow times the driving potential gradient, which is proportional to entropy production during steady states (Eq. 4).

Additionally, we calculated power production using data from a numerical experiment carried out in the study of Zehe et al. (2010). They simulated soil water dynamics and surface runoff response to a block rain of 10 mm h^{-1} for a selected field site in the meadow close to the Weiherbach. Total simulation period was one day. The stretch was 30 m long, 2 m deep, total elevation difference was 2 m. Soil hydraulic properties of the apparent Colluvisol are listed in Table 1. As the lateral grid width was 2 cm, vertical worm burrows were represented as explicit connected structures in the model domain (Fig. 4d). Maximum water flow rates in a single worm burrow exceeded the value of the soil matrix by a factor of 100. In the present study we re-analyzed simulation results for 5, 10, 15, 20 and 25 burrows m^{-2} by calculating power (from Eq. 4) in soil water flow (SW), ground water recharge (GW) and overland flow (OFL) per time step by numerically integrating the product of flow and the gradient across the entire model domain/boundaries. Additionally, we plotted power production averaged over the 1 day long simulation period as a function of the areal worm burrow density. This is an additional test of hypothesis H1, but for vertically connected macropores at the small field scale and for a single event. Note that in the following we will always normalize power production and free energy with the surface area of either the hillslope or the catchment under investigation.

HESSD
9, 10595–10655, 2012

3.3.2 Experiment 2: is there an optimal macropore density in the Weiherbach soils?

In the second numerical experiment we used the basic model setup (Case 1 of experiment 1) but gradually increased macroporosity f_m from 1 to a maximum of 4.2 within 30 steps for a single representative hillslope. According to Eq. (13), this gradual increase corresponds to a higher maximum infiltrability and implies a higher density of activated macropores/worm burrows. Zehe et al. (2010) have already corroborated that an elevated density of worm burrows enhances the dissipation of free energy during single rainfall events. Their study focused exclusively, however, on free energy dynamics as determined by the first term in Eq. (12). Within the present study we account for the trade-off arising from the amount of water that is stored in the soil, which dissipates free energy by depleting gradients in soil water potentials, and water export from the system, which exports free energy by means of ground water recharge and surface runoff. The numerical experiment shall thus reveal whether this trade-off leads to an optimum macroporosity. We thus calculated power (from Eq. 4) in soil water flow (SW), ground water recharge (GW) and overland flow (OFL) per time step by numerical integration across the entire model boundaries. Similarly, we integrated Eq. (12) for each time step to calculate free energy in the entire model domain. We then checked whether there is a macroporosity factor that maximizes entropy production averaged across the entire simulation period, or that maximized free energy reduction/dissipation over the simulation period. The latter was calculated by subtracting free energy at the end of the simulation from its initial value.

The next idea was to assign this thermodynamically optimal macroporosity factor – if existent – to all 169 hillslopes of the catchment, simulate the catchment scale water balance and compare simulation results with those of the best fit as well as to the observed runoff behavior.

HESSD
9, 10595–10655, 2012

3.3.3 Experiment 3: what is the optimal hillslope architecture given a fixed macroporosity?

In the last numerical experiment for the Weiherbach we simulated the water balance for the period from 21 April 1994 to 15 September 1995 for:

- Case 1: the basic model setup based on the typical catena, spatially organized macroporosity and the f_m value that yielded the best fit (1.5);
- Case 2: the basic model setup but with a flipped spatial pattern of macroporosity (decreasing macroporosity with slope length). Note: this implies that ecosystem engineers with a different habitat preference have created the opposite spatial pattern of preferential pathways, because they prefer a drier soil habitat;
- Case 3: the basic setup with a flipped spatial pattern of macroporosity and a flipped catena. We admit that this appears to be a non-meaningful scenario with respect to the discussion in the introduction. It implies that fine material has been left as residuals in the hilltop area, while it has been washed away in the hill foot reaches, leaving coarser materials there. Additionally, we assume that anecic worms which prefer the upslope fine grained soils have built the preferential pathways.

Note that within these procedure we changed neither the relative fraction of the respective soil types, nor the fraction of hillslope reaches that have high, medium or low macroporosity, nor absolute values of f_m. This implies that (a) averages, (b) variance and (c) covariance of hydraulic properties remain invariant. What does change, however, is their topology, i.e. their sequence along the direction of the potential gradient that drives overland flow downslope.

HESSD
9, 10595–10655, 2012

3.3.4 Experiment 4: is there an optimal macropore density in young ash soils of the Malalcahuello catchment?

For the Malalcahuello we just performed the analogue to experiment 2 to explore the existence of an optimal macroporosity factor. As the basic model setup for the Malalcahuello catchment is not based on a similar clear spatial organization of soils and macropores at the hillslope scale as in the Weiherbach, the analogue to experiment 3 does not make sense here.

We gradually increased macroporosity from 1 to a maximum of 70 within 20 steps. Then we calculated power in soil water fluxes in the domain as well as in the other fluxes leaving the domain from Eq. (4) as well the trajectories of total free energy from Eq. (12). Finally we checked whether there is a macroporosity factor that maximizes average entropy production/ power in the entire simulation period or minimized free energy at the end of the simulation period, which was the half year long snow-free period in 2004. Each model run was dynamically initialized allowing for a spin up of 1 yr.

4 Results

4.1 Numerical experiment 1: river networks accelerate entropy production

Figure 5 presents total accumulated runoff simulated with the three catchment configurations (panel a). Accumulated runoff for case 1 (recent catchment geomorphology) at the end of the simulation is more than ten times larger than for the other cases. This is because the two other geomorphologies can due to the absence of the river network and not produce a base flow component. Event-scale surface runoff responses for the largest observed runoff event and the corresponding rainfall forcing are shown in Fig. 5d and b, respectively. Simulated event-scale runoff and thus power generation is 50 % larger for case 1 when compared to cases 2 and 3. This is because power

HESSD
9, 10595–10655, 2012

generation/ entropy production adjusts linearly (due to Eq. 4) with the runoff /discharge loss from the catchments (Fig. 5c). Note that case 3 (solid black in panels c and d), i.e. when the hillslope of the same size, length, total elevation difference and catena as the catchment, is shaped according to the hypsometric curve, is only slightly more efficient in generating power/producing entropy, as the linear slope in case 2. As accumulated kinetic energy export increases directly with accumulated total runoff, it is more than ten times larger in case 1 than in the other two cases. This is mainly due to the base flow component that creates memory in the kinetic energy export. This point will be further elaborated in the discussion section.

These results suggest that a change from a linear shaped catchment to a mature geomorphology does – without additional formation of a river net – only slightly increase runoff and thus reduction of free energy by means of kinetic energy export. The additional formation of a connected river, which implies of course also that there are locally steepened hillslopes in the vicinity of the stream of low stream order, causes in contrast a strongly enhanced entropy production and export of free energy. The simulation results from numerical experiment 1 thus corroborate the hypothesis H2 that a connected river net enhances power generation and thus entropy production, both at the time of the event and on the seasonal time scale.

Figure 6 presents fluxes of the cumulated water balance (panel a) of the hillslope stretch: accumulated block rain (solid red), evapotranspiration (solid blue) and cumulated surface runoff in solid green. Overland flow response decreases as expected with increasing areal density of macropores both in volume (panel a) and in peak height (panel c). Power generation is dominated by soil water flows (panel b) and reaches up to $10\,W\,m^{-2}$ during rainfall and decreases by two orders of magnitude at the end of the experiment. But also overland flow has a small contribution that peaks at $0.5\,W\,m^{-2}$. Power generation averaged over one day increases almost linearly with areal density of macropores. This is explained by the strong enhancement of infiltrability by a factor of more than 1000, and the strongly enhanced flow against the gradient in soil hydraulic potential. Again this finding corroborates hypothesis H1.

HESSD
9, 10595–10655, 2012

Average power generation in overland flow is also increasing with increasing density of macropores. As surface runoff volume is not only controlled by the density but also by the actual position of the macropores at the hillslope (which is random here), this is not a strongly monotonous decrease in the present case. The next section will show that overland flow and thus generated power does decrease monotonously with decreasing macroporosity when its spatial pattern is fixed.

4.2 Numerical experiment 2: search for an optimum macroporosity in the Weiherbach soils?

The accumulated fluxes of the water balance of the selected hillslope corroborate the rareness of rainfall runoff events in the Weiherbach (Fig. 7a). The water balance is dominated by evapo-transpiration (solid blue), followed by ground water recharge (dashed red) and occasional surface runoff events. Different macroporosity values have thus only a marginal effect on the water balance. Nevertheless, event scale overland flow is strongly reduced by an increasing macroporosity as exemplarily shown for the largest rainfall event observed at 27 June 1994 (Fig. 7b).

Figure 8 presents time series of different forms of free energy (panel a) and power produced by different water flow components (panel b). Soil water flows dominate power generation (solid red) and thus entropy production compared to power generation by groundwater recharge (solid green) and by means of overland flow events (solid blue). This is because soil water flows especially during dry spells and near the soil surface against the steepest potential gradient. Maximum values of power in soil water flows thus reach up to $100\,\mathrm{W\,m^{-2}}$; higher macroporosity factors accelerate infiltration and thus depletion of these potential gradients. Run number 8, with a corresponding f_m of 1.7, maximises total power generation and thus entropy production averaged over the entire simulation period (panel d). Depletion of a matric potential is due to the non-linear shape of the soil water retention curve a non-linear phenomenon: a small increase in soil water content can strongly decrease the absolute value of matric potentials. An additional increase in infiltration by a higher macroporosity and thus infiltrability

HESSD
9, 10595–10655, 2012

can thus be compensated by a strong reduction in the potential gradient. This, together with the dominance of soil water flows, explains the existence of the relatively sharp maximum.

Figure 8b presents the time series of different forms of free energy computed by means of Eq. (9). Capillary binding energy makes in these fine porous soils by far the largest contribution to total free energy dynamics compared to potential energy. But also kinetic energy export (solid green, negative) has – at least during strong rainfall events – a clear contribution to free energy dynamics. Run 7, with an f_m value of 1.6, maximises free energy reduction/dissipation over the simulation period (panel d). Hence, both maximum power generation/entropy production (MEP) and free energy dissipation/reduction (MED Maximum Energy Dissipation) suggest slightly different optimal hillslope scale macroporosity factors. In the discussion section we will provide a possible explanation for this difference.

Figure 7d compares simulated catchment scale discharge based on these optimal hillslope architectures (MEP in solid red, MED in dashed red) to results of the best fit setup (macroporosity of 1.5, solid blue) and the discharge response observed at 27 June 1994. In particular, the simulation based on the MED optimum is in reasonable accordance with observed discharge when compared to the best fit.

4.3 Numerical experiment 3: spatial re-organization of patterns in the Weiherbach

Simulated catchment scale discharge (Fig. 9a and b) during experiment 3 was 60 % for the observed hillslope architecture (Case 1) when compared to Case 2 (spatially flipped pattern of macroporosity) and even 50 % when compared to Case 3 (when both patterns are flipped in space). In consequence, total free energy at the end of the 1.5 yr long simulation period was clearly smaller for case 1 for the spatially "re-organized" macroporosity patterns (Fig. 9d). In fact total free energy is clearly smaller for Case 1 as for Case 2 during almost the entire simulation period. Note that both cases are identical with respect to mean, variance and covariance lengths of both macroporosity

HESSD
9, 10595–10655, 2012

and soil hydraulic properties. They differ with respect to the spatial cross-covariance of macroporosity and soil hydraulic functions at the hillslope scale and with respect to the arrangement of the pattern of macroporosity along the macroscale lateral potential gradient. Case 1 and Case 3 are even identical with respect to the cross-covariance of macroporosity and soil hydraulic properties. The only difference is in the arrangement of these different "functional units", in this case sectors with homogeneous functional soil parameters and macroporosity, along the macroscale lateral potential gradient. This different topological arrangement has however a clear influence on overland hillslope flow and catchment scale overland response and free energy dynamics.

4.4 Numerical experiment 4: Malalcahuello catchment

The accumulated fluxes of the water balance of the hillslope corroborate that runoff generation in the Malalcahuello catchment functions totally differently when compared to the Weiherbach (Fig. 10a). Accumulated rainfall (solid red) is twice as large compared to the Weiherbach, though the simulation period is just half as long. For a small macroporosity the simulated water balance is dominated by groundwater recharge, followed by subsurface storm flow. At large macroporosity values subsurface storm flow plays the dominant part. The best fit of observed specific discharge (Nash Sutcliffe efficiency 0.7) was achieved with a macroporosity factor of 54 (Panel c, observed runoff is in solid blue).

Free energy dynamics and power generation in the Malalcahuello catchment is dominated by different water flows when compared to the Weiherbach catchment. Capillary binding energy is less strong in these young, coarse grained volcanic ash soils. Matric potential gradients in soil are thus much flatter and total free energy dynamics in soil is dominated by dynamics in potential energy (not shown here). Ground water recharge (GW) and subsurface storm flow (SSF) dominate power generation and depletion of gradients. SSF dominates at the event scale with maximum values of $100\,\mathrm{W\,m^{-2}}$. GW-recharge dominates as a slowly varying component at the seasonal scale and is one order of magnitude larger than in the Weiherbach catchment. In contrast to the

HESSD
9, 10595–10655, 2012

Weiherbach, there is no apparent optimum, neither a maximum in average power generation (Fig. 10d) nor a maximum in free energy reduction during the simulation period (not shown). As overland flow has no influence here, there is no trade-off between infiltration and overland flow production as in the Weiherbach. An increasing macroporosity enhances flow against driving gradients in soil, increases the ratio between SSF and GW recharge and thus enhances total specific runoff (panel c). Thus power generation in GW recharge is decreasing while power generation in subsurface storm flow is increasing with increasing macroporosity. The net result is that averaged total power increases with macroporosity (panel d).

5 Discussion and conclusions

5.1 Flow networks as dissipative structures

The first numerical experiment corroborates that overland flow in connected river networks is clearly accelerated when compared to sheet flow. Simulated overland flow production for the "catchment size" hillslope, which had the same size, length, total elevation difference, catena, spatial patterns of macroporosity and landuse as the Weiherbach catchment and was shaped according to the hypsometric curve, was reduced by almost 50 %. The shape of these "catchment size" hillslopes was shown to be of marginal importance since runoff from the mature sigmoid type was only slightly enhanced when compared to a linear homogeneous catchment size slope. This suggests that an evolution of a catchment towards an architecture that enhances runoff implies co-evolution of linear slopes to mature sigmoid types and of a river network (with locally steepened river banks) that interconnects these mature hillslopes. Enhanced runoff implies more efficient dissipation of free energy by means of kinetic energy export, enhanced power generation and entropy production. We conclude that numerical experiment 1 does clearly support hypothesis H2 and highlights that the formation of

HESSD
9, 10595–10655, 2012

connected river networks makes a qualitative difference with respect to accelerating runoff and enhancing power generation/entropy production.

The reanalysis of the numerical experiment 1 of the study of Zehe et al. (2010) further supports hypothesis H1. An elevated density of vertical macropores increases flow against soil water potential gradients during a simulated block rain of 10 mm in 1 h. Power production does linearly increase with macropore density. Also vertical worm burrows do thus act as dissipative structures. At this small field stretch we did not find an optimum macropore density. This can be explained (a) by the ten times smaller topographic gradient (2 m/30 m), therefore the trade-off between kinetic energy export by means of overland flow and depletion of soil water potential gradients is not that strong; and (b) by the small time scale for analyzing power generation. Averaging across a single event is not enough to characterize steady state behaviour with respect to power generation and production of entropy.

We conclude that river networks are a prime example for macroscale dissipative structures, which would enhance dissipation and depletion of apparent macroscale potential gradients, if rainfall did not always re-establish this gradient (compare Sect. 2.1). Note that enhancement of macroscale dissipation of free energy is a consequence of reducing local dissipation/friction per unit mass transported in the river net (Kleidon et al., 2012). Minimum energy expenditure (Rodriguez-Iturbe and Rinaldo, 2001) and Maximum Power/MEP do thus not contradict each other but arise from different scale perspectives.

The significance of the river net is that it creates memory in overland flow in the form of base flow and due to the high flow velocity in the river memory in kinetic energy export. Accumulated total runoff in case 1 (catchment with recent geomorphology) was 150 mm due to apparent base flow. This corresponds to (a) the long term average specific discharge observed at gauge Menzingen and (b) to the accumulated ground water recharge simulated in the cases 2 and 3. Let's assume that groundwater recharge (150 mm yr^{-1}) in these two cases feeds steady state groundwater runoff. The accumulated 150 mm yr^{-1} specific runoff volume corresponds to 0.016 m^3 s^{-1} average

HESSD
9, 10595–10655, 2012

base flow of the Weiherbach at gauge Menzingen. This has to be equal to groundwater runoff in cases 2 and 3 during steady state conditions. Let's now assume a hydraulic conductivity of the aquifer of 10^{-4} m s^{-1}; which is 100–1000 times larger than the saturated hydraulic conductivity in the deep unsaturated Loess layers (Zehe et al., 2001) in the Weiherbach. If we assume a hydraulic head gradient equal to the average topographic gradient in cases 2 and 3 (40 m/2000 m), we can estimate the aquifer cross-sectional area that is necessary to allow such steady state groundwater runoff to leave the catchment as 8300 m^2. As the width of the two uniform catchment sized hillslopes is 1750 m, the necessary aquifer thickness is 4.7 m. If we assume that the steady hydraulic gradient driving this hypothetical groundwater runoff is one order of magnitude smaller (more realistic), we have either to assume a ten times larger aquifer thickness or a hydraulic conductivity of 10^{-3} m s^{-1}, which implies in our perception the presence of connected structures in the aquifer. From this simple calculation we conclude that the present steady state water cycle in the Weiherbach (and also in larger catchments) could not function without connected structures – either the river network or fractures that facilitated drainage of excess water. This corroborates our initial statement that textural elements are storage elements not drainage elements in the landscape.

5.2 Thermodynamic optimal hillslope architectures for the Weiherbach: coincidence or co-evolution?

Results from numerical experiments 2 and 3 suggest, as far as we are aware for the first time, that the spatially organized patterns of soils and vertical macropores that have been observed in a real world landscape (the Weiherbach) are in close accordance with a thermodynamic optimum. This holds for both the macroporosity, which represents the enhancement of infiltration by activated macropores per unit area, and the spatially arrangement of these patterns along the driving lateral potential gradient at the hillslope scale.

HESSD
9, 10595–10655, 2012

5.2.1 Optimal macroporosity in mature Loess soils

In numerical experiment 2 we found very similar macroporosity factors which maximized average power generation (1.7) or maximized free energy reduction (1.6) within the simulation period. These optima arise from the trade-off between depleting matric potential gradients by enhanced infiltration and export of kinetic energy by means of overland flow. As already mentioned, depletion of a matric potential gradient is a non-linear phenomenon: a small increase in soil water content can strongly decrease the absolute value of near surface matric potentials. An additional increase in infiltration by enlarging the macroporosity and thus infiltrability is at higher water contents compensated by a reduction/flattening of near surface matric potential gradients. Entropy production by soil water flows and free energy dissipation does thus not further increase with increasing macroporosity when this "break-even point" is exceeded, while kinetic energy export still decreases due to a reduction in surface runoff.

This trade-off limits the degree to which a higher amount of active macropores, which are in the Weiherbach created by anecic earthworms, increases the efficiency of the system to produce entropy/dissipate free energy during steady state conditions. It is striking that these hillslope scale optima were close to the "best fit macroporosity (1.5)" and simulated catchment scale discharge based on these optima was in reasonable accordance with observed discharge response; in fact, they were close to the best fit. Why are these different optima close but not identical? This can be explained by the fact that free energy reduction also accounts for the effect of evapo-transpiration (ET), which enlarges matric potentials during dry spells. Power generation by means of ET was – as explained in the introduction – not included in the calculation of overall power generation. The MED optimum can thus be deemed as being closer to the overall optimum, while the MEP optimum accounts exclusively for the trade-off arising from flows of liquid water: soil water flow, ground water recharges and surface runoff.

We conclude that the results from numerical experiment 2 fully support hypothesis H2 and its implications I2 and I3, which state that recent systems should be very

HESSD
9, 10595–10655, 2012

efficient in reducing free energy (by depletion of gradients and free energy export) and close to the optimum (when existent). We hypothesize that the thermodynamic optimum macroporosity, which reflects the areal density of worm burrows and is related to the abundance of anecic earthworms, is not beyond a value that can, given the biotic and ecological limitations, establish in this landscape. The small deviation of the best fit from the optimum might be explained due to disturbances from agricultural practice. Testing of such a hypothesis requires development of coupled models for hydrology and population dynamics of earthworms, or in general terms, of models that account for the relevant interactions and feedbacks between biotic and abiotic processes and limitations for biotic structure formation and their controls on water fluxes.

5.2.2 Recent spatial arrangement of patterns is optimal

Numerical experiment 3 corroborates furthermore that (a) the typical erosion catena and (b) pattern of worm burrow densities which reflect the habitat preference of the main ecosystem engineers are most efficient in dissipating free energy. This typical catena with accumulated fine materials at the hill foot sectors is a fingerprint of past dissipative processes. Higher worm burrow densities downslope reflect their habitat preference for moist but drained Colluvisols and thus rather ecological than thermodynamic optimality. Note that the different scenarios in experiment 3 assume either (a) that ecosystem engineers with a (different) habitat preference for drier soils dominate macropore formation, or (b) that fine material has been left over at hilltops (which is not a meaningful but an instructive scenario). Each of these hypothetical forms of spatial organization has been shown to produce more overland flow and be less efficient in reducing free energy of the system within the 1.5 yr long simulation. This implies that the reorganized systems are on average further away from a thermodynamic equilibrium state of minimum free energy.

We thus conclude that the real spatial patterns, which co-evolved in response to past dissipative processes, is indeed functionally superior in the sense of H2, when compared to other spatially organized patterns. This finding clearly supports hypothesis

HESSD
9, 10595–10655, 2012

H2 and its implications I2 and I3. We suggest that the spatial organization of functional units (soils types and vertical connected macropore networks), i.e. their spatial arrangement along a superordinate potential gradient, is not a random product but the result of co-evolution towards a configuration that increases dissipation of free energy, possibly towards an optimum, when existent. This is favourable for fast relaxation towards thermodynamic equilibrium, which implies faster redistribution of water in soil (reducing mechanical stressors) and fast export of excess water and is thus favourable for (mechanic) stability of the system against frequent disturbances due to large precipitation events. Ecosystem engineers whose biotic optimal pattern of soil structures is opposite to the thermodynamic optimum will, in contrast, weaken their habitat which can be deemed to be selection criteria against these species.

5.3 Maximum drainage as optimum in young volcanic ash soils

In the case of the Malalcahuello catchment we did not find a macroporosity factor that maximized total power generation/ free energy reduction at the end of the simulation period. In this young, highly permeable volcanic ash soils, runoff production is dominated by base flow and subsurface storm flow from the lower hillslope sectors; overland flow does not occur (Blume et al., 2007). Soil water flow, due to the low water retention properties and flatter near surface matric potential gradients, plays a minor role in power generation and entropy production. Free energy dynamics are dominated by potential energy in soil. The latter is, however, minimized by maximizing drainage. Consequently, average power generation continuously increased and free energy at the end of the simulation time continuously decreased with increasing macroporosity. Even at a macroporosity factor of 70 (run 20), which corresponds to maximum flow velocities in the macroporous layer of almost $10^{-2}\,m\,s^{-1}$, there was no detectable plateau in power generation. The macroporosity factor that yielded a best fit of the observed specific discharge (NSE 0.7) was, at 54, remarkably high and corresponds to an infiltrability of $10^{-3}\,m\,s^{-1}$ (compare Table 2). This finding does at least not contradict H2 and its implication I3.

HESSD
9, 10595–10655, 2012

Vertical preferential flow in these non-cohesive soils is, according to Blume et al. (2009), not classical flow in connected macropores but is the result of wetting front instabilities and formation of hydrophilic channels in a hydrophobic matrix in summer. We thus conclude that in such a hydro-pedological setting without water limitation (annual rainfall is 3000 mm) and at this stage of soil formation and ecosystem evolution, enlargement of drainage seems to be favorable as it increases power reduction in free energy dynamics.

6 Summary and overall conclusions

In summary we state that the present study establishes, as far as we know, for the first time a thoroughly detailed link between hydrological dynamics and thermodynamics. Based on this theory we may shed light on the dynamics and dissipation of free energy and production of entropy in the critical zone by analyzing simulated dynamics from physically based hydrological models. This is exemplified in the Weiherbach and the Malalcahuello catchment which are located in strongly different hydro-climactic and hydro-pedological settings. The application to the Weiherbach catchment suggests the existence of thermodynamic optimal hillslope structures as a result of co-evolution of biotic patterns and the soil catena. These optima allow acceptable uncalibrated reproduction of observed rainfall-runoff behaviour when being used in a catchment model: in fact they come close to the best fit. Application showed furthermore that connected networks like vertical preferential pathways and the river net, act as dissipative structures by accelerating flow against driving gradients, which implies an elevated entropy production. This seems to be “a key instrument in this concert”.

We conclude that this theory makes a substantial contribution to understanding the omnipresence of preferential flow and the functional advantage of this phenomenon; which seems to be independent of scale and nature of the flow paths. Although we did not address biotic structure formation in an explicit manner we think this

HESSD
9, 10595–10655, 2012

can be accounted for in the presented framework (we need the right models) as well as the trade-off between short and long term dynamics.

We conclude further that the presented findings are promising for predictions in ungauged catchments (PUB). The thermodynamic optimal model structure can, if existent, be used as first guess for an uncalibrated simulation of rainfall runoff. In case of the Weiherbach catchment this uncalibrated simulation of catchment scale overland flow is not the best but a good match of the observed discharge time series over 1.5 yr. For the Malalcahuello catchment it seems that maximum drainage is the optimum: this provides at least the clue as to how to tune the model. The proposed thermodynamic treatment does however require physically consistent models, i.e. that flows are driven by potential gradients, as explained in Sect. 2.2.

In general it seems necessary to explore the full concert of processes, including evaporation and the underlying structural and biotic controls, in such an optimization. This is, however, not a straightforward issue. For instance, we cannot assume that the photosynthetically active vegetation biomass will be elevated by 20 %, without checking whether this could be possible with the given nutrient, water and energy resources. Even if possible, such a transition does not happen overnight and feeds back to litter fall, habitat for resident organisms and thus soil structures controlling other processes. Also, reshuffling of soil and functional vegetation in pristine areas is not a meaningful scenario, as soils, soil biota and soil structures co-evolved, influenced by litter fall, throughfall, etc. In contrary, in agricultural systems this makes sense as most soils and soil biota have experienced typical arable crops and related management techniques several times.

Accounting for the full concert of processes in such a treatment requires coupled models for hydrology, population dynamics of ecosystem engineers and the most important vegetation that account for the key interactions, feedbacks and factors that (a) limit biotic structure formation and (b) stationary vegetation biomass and thus pose upper limits to infiltrability and plant transpiration. As these models are currently not at hand, one has as in the present case or in the study of Porada et al. (2011) to

HESSD
9, 10595–10655, 2012

optimize model parameters for individual processes under constraints, for instance by fixing the water balance. A naïve, free optimization of a model structure to maximise power/entropy production will simply maximize the water flow against the steepest gradient, which is transpiration. An ecosystem configuration that maximizes transpiration is, however, unlikely as a steady state configuration: it will end up as a desert.

Acknowledgements. We sincerely thank the German Research Foundation (DFG) as part of this research has been funded in the frame of the CAOS Research Unit (FOR 1598) as well as in the BIOPORE Project (ZE 533/5-1). We acknowledge support by Deutsche Forschungsgemeinschaft and Open Access Publishing Fund of Karlsruhe Institute of Technology.

The service charges for this open access publication have been covered by a Research Centre of the Helmholtz Association.

References

Bejan, A.: Constructal theory of pattern formation, Hydrol. Earth Syst. Sci., 11, 753–768, doi:10.5194/hess-11-753-2007, 2007.

Bejan, A., Lorente, S., and Lee, J.: Unifying constructal theory of tree roots, canopies and forests, J. Theor. Biol., 254, 529–540, doi:10.1016/j.jtbi.2008.06.026, 2008.

Beven, K. and Germann, K.: Macropores and water flow in soils, Water Resour. Res., 18, 1311–1325, 1982.

Beven, K. and Clarke, R. T.: On the variation of infiltration into a soil matrix containing a population of macropores, Water Resour. Res., 22, 383–385, 1986.

Bloschl, G. and Sivapalan, M.: Scale Issues In Hydrological Modeling – A Review, Hydrol. Process., 9, 251–290, 1995.

Blume, T., Zehe, E., and Bronstert, A.: Rainfall-runoff response, event-based runoff coefficients and hydrograph separation, Hydrolog. Sci. J., 52, 843–862, 2007.

Blume, T.: Hydrological processes in volcanic ash soils : measuring, modelling and understanding runoff generation in an undisturbed catchment, Ph. D., Institut für Geoökologie, Universität Potsdam, Potsdam, 153 pp., 2008.

HESSD

9, 10595–10655, 2012

Blume, T., Zehe, E., and Bronstert, A.: Investigation of runoff generation in a pristine, poorly gauged catchment in the Chilean Andes II: Qualitative and quantitative use of tracers at three spatial scales, Hydrol. Process., 22, 3676–3688, doi:10.1002/hyp.6970, 2008a.

Blume, T., Zehe, E., Reusser, D. E., Iroume, A., and Bronstert, A.: Investigation of runoff generation in a pristine, poorly gauged catchment in the Chilean Andes I: A multi-method experimental study, Hydrolog. Process., 22, 3661–3675, doi:10.1002/hyp.6971, 2008b.

Blume, T., Zehe, E., and Bronstert, A.: Use of soil moisture dynamics and patterns at different spatio-temporal scales for the investigation of subsurface flow processes, Hydrol. Earth Syst. Sci., 13, 1215–1233, doi:10.5194/hess-13-1215-2009, 2009.

Bull, L. J. and Kirkby, M. J.: Gully processes and modelling, Prog. Phys. Geog., 21, 354–374, 1997.

Celia, M. A. and Bouloutas, E. T.: A general mass-conservative numerical solution for the unsaturated flow equation, Water Resour. Res., 26, 483–1496, 1990.

Dietrich, W. E. and Perron, J. T.: The search for a topographic signature of life, Nature, 439, 411–418, 2006.

Dooge, J. C. I.: Looking for hydrological laws, Water Resour. Res., 22, 46S–58S, 1986.

Ehlers, W., Avci, O., and Markert, B.: Computation of Slope Movements Initiated by Rain-Induced Shear Bands in Small-Scale Tests and In Situ, Vadose Zone J., 10, 512–525, doi:10.2136/vzj2009.0156, 2011.

Hinkelmann, R., Zehe, E., Ehlers, W., and Joswig, M.: Special Section on Landslides: Setting the Scene and Outline of Contributing Studies, Vadose Zone J., 10, 473–476, doi:10.2136/vzj2011.0032, 2011.

Howard, A. D.: Theoretical model of optimal drainage networks, Water Resour. Res., 26, 2107–2117, 1990.

Kirkby, M. J., Bull, L. J., Poesen, J., Nachtergaele, J., and Vandekerckhove, L.: Observed and modelled distributions of channel and gully heads – with examples from SE Spain and Belgium, Catena, 50, 415–434, 2003.

Klaus, J. and Zehe, E.: Modelling rapid flow response of a tile drained field site using a 2D-physically based model: assessment of "equifinal" model setups, Hydrolog. Process., 24, 1595–1609, doi:10.1002/hyp.7687, 2010.

Klaus, J. and Zehe, E.: A novel explicit approach to model bromide and pesticide transport in connected soil structures, Hydrol. Earth Syst. Sci., 15, 2127–2144, doi:10.5194/hess-15-2127-2011, 2011.

HESSD
9, 10595–10655, 2012

Kleidon, A., Fraedrich, K., Kirk, E., and Lunkeit, F.: Maximum entropy production and the strength of boundary layer exchange in an atmospheric general circulation model, Geophys. Res. Lett., 33, L06706, doi:10.1029/2005gl025373, 2006.
Kleidon, A. and Schymanski, S.: Thermodynamics and optimality of the water budget on land: A review, Geophys. Res. Lett., 35, L20404, doi:10.1029/2008gl035393, 2008.
Kleidon, A., Zehe, E., Ehret, U., and Scherer, U.: Thermodynamics, maximum power, and the dynamics of preferential river flow structures on continents, Hydrol. Earth Syst. Sci. Discuss., 9, 7317–7378, doi:10.5194/hessd-9-7317-2012, 2012.
Kondepudi, D. and Prigogine, I.: Modern Thermodynamics: From Heat Engines to Dissipative Structures, John Wiley Chichester, UK, 1998.
Lee, H., Zehe, E., and Sivapalan, M.: Predictions of rainfall-runoff response and soil moisture dynamics in a microscale catchment using the CREW model, Hydrol. Earth Syst. Sci., 11, 819–849, doi:10.5194/hess-11-819-2007, 2007.
Lindenmaier, F., Zehe, E., Dittfurth, A., and Ihringer, J.: Process identification on a slow moving landslide, Hydrolog. Process., 19, 1635–1651, 2005.
Lorenz, R. D., Lunine, J. I., Withers, P. G., and McKay, C. P.: Titan, Mars and Earth: Entropy production by latitudinal heat transport, Geophys. Res. Lett., 28, 415–418, 2001.
Lotka, A. J.: Contribution to the energetics of evolution, Proc. Natl. Acad. Sci. USA, 8, 147–151, 1922a.
Lotka, A. J.: Natural selection as a physical principle, Proc. Natl. Acad. Sci. USA, 8, 151–154, 1922b.
Mualem, Y.: A new model for predicting the hydraulic conductivity of unsaturated porous media, Water Resour. Res., 12, 513–522, 1976.
Odum, E. P.: The strategy of ecosystem development, Science, 164, 262–270, 1969.
Parkner, T., Page, M., Marden, M., and Marutani, T.: Gully systems under undisturbed indigenous forest, East Coast Region, New Zealand, Geomorphology, 84, 241–253, doi:10.1016/j.geomorph.2006.01.042, 2007.
Phillips, J. D.: Evolutionary geomorphology: thresholds and nonlinearity in landform response to environmental change, Hydrol. Earth Syst. Sci., 10, 731–742, doi:10.5194/hess-10-731-2006, 2006.
Poesen, J., Nachtergaele, J., Verstraeten, G., and Valentin, C.: Gully erosion and environmental change: importance and research needs, Catena, 50, 91–133, 2003.

HESSD
9, 10595–10655, 2012

Porada, P., Kleidon, A., and Schymanski, S. J.: Entropy production of soil hydrological processes and its maximisation, Earth Syst. Dynam., 2, 179–190, doi:10.5194/esd-2-179-2011, 2011.
Reggiani, P., Hassanizadeh, S. M., and Sivapalan, M.: A unifying framework for watershed thermodynamics: balance equations for mass, momentum, energy and entropy, and the second law of thermodynamics, Adv. Water Resour., 22, 367–398, 1998.
Rinaldo, A., Maritan, A., Colaiori, F., Flammini, A., and Rigon, R.: Thermodynamics of fractal networks, Phys. Rev. Lett., 76, 3364–3367, 1996.
Rodriguez-Iturbe, I., D'Odorico, P., and Rinaldo, A.: Configuration entropy of fractal landscapes, Geophys. Res. Lett., 25, 1015–1018, 1998.
Rodriguez-Iturbe, I. and Rinaldo, A.: Fractal River Basins: Chance and Self-Organization, Cambridge Univ. Press, Cambridge, UK, 2001.
Scherer, U., Zehe, E., Trabing, K., and Gerlinger, K.: Prediction of soil detachment in agricultural loess catchments: Model development and parameterisation, Catena, 90, 63–75, doi:10.1016/j.catena.2011.11.003, 2012.
Schulz, K., Seppelt, R., Zehe, E., Vogel, H.-J., and Attinger, S.: Importance of spatial structures in advancing hydrological sciences, Water Resour. Res., 42, W03S03, doi:10.1029/2005WR004301, 2006.
Shao, X. J., Wang, H., and Hu, H. W.: Experimental and modeling approach to the study of the critical slope for the initiation of rill flow erosion, Water Resour. Res., 41, W12405, doi:10.1029/2005wr003991, 2005.
Uhlenbrook, S.: Catchment hydrology - a science in which all processes are preferential – Invited commentary, Hydrolog. Process., 20, 3581–3585, doi:10.1002/hyp.6564, 2006.
van Genuchten, M. T.: A closed-form equation for predicting the hydraulic conductivity of unsaturated soils, Soil Sci. Soc. Am. Jour., 44, 892–898, 1980.
Vogel, H.-J., Hoffmann H., and Roth, K.: Studies of crack dynamics in clay soil I: Experimental methods, results and morphological quantification, Geoderma, 125, 203–211, 2005.
Weiler, M. and McDonnell, J. J.: Conceptualizing lateral preferential flow and flow networks and simulating the effects on gauged and ungauged hillslopes, Water Resour. Res., 43, W0340310, doi:10.1029/2006wr004867, 2007.
Wienhofer, J., Lindenmaier, F., and Zehe, E.: Challenges in Understanding the Hydrologic Controls on the Mobility of Slow-Moving Landslides, Vadose Zone J., 10, 496–511, doi:10.2136/vzj2009.0182, 2011.

HESSD
9, 10595–10655, 2012

Wienhöfer, J., Germer, K., Lindenmaier, F., Färber, A., and Zehe, E.: Applied tracers for the observation of subsurface stormflow at the hillslope scale, Hydrol. Earth Syst. Sci., 13, 1145–1161, doi:10.5194/hess-13-1145-2009, 2009.

Zehe, E.: Stofftransport in der ungesättigten Bodenzone auf verschiedenen Skalen, Institut für Hydrologie und Wasserwirtschaft, Mitteilungen des Instituts für Hydrologie und Wasserwirtschaft, Universität Karlsruhe (TH), Karlsruhe, 227 pp., 1999.

Zehe, E. and Fluhler, H.: Slope scale variation of flow patterns in soil profiles, J. Hydrol., 247, 116–132, 2001.

Zehe, E., Maurer, T., Ihringer, J., and Plate, E.: Modelling water flow and mass transport in a Loess catchment, Phys. Chem. Earth (B), 26, 487–507, 2001.

Zehe, E. and Bloeschl, G.: Predictability of hydrologic response at the plot and catchment scales – the role of initial conditions, Water Resour. Res., 40, W10202, doi:10.1029/2003WR002869, 2004.

Zehe, E., Becker, R., Bardossy, A., and Plate, E.: Uncertainty of simulated catchment runoff response in the presence of threshold processes: Role of initial soil moisture and precipitation, J. Hydrol., 315, 183–202, 2005.

Zehe, E., Lee, H., and Sivapalan, M.: Dynamical process upscaling for deriving catchment scale state variables and constitutive relations for meso-scale process models, Hydrol. Earth Syst. Sci., 10, 981–996, doi:10.5194/hess-10-981-2006, 2006.

Zehe, E., Elsenbeer, H., Lindenmaier, F., Schulz, K., and Bloschl, G.: Patterns of predictability in hydrological threshold systems, Water Resour. Res., 43, W07434, doi:10.1029/2006wr005589, 2007.

Zehe, E. and Sivapalan, M.: Threshold behaviour in hydrological systems as (human) geo-ecosystems: manifestations, controls, implications, Hydrol. Earth Syst. Sci., 13, 1273–1297, doi:10.5194/hess-13-1273-2009, 2009.

Zehe, E., Blume, T., and Blöschl, G.: The principle of "maximum energy dissipation": a novel thermodynamic perspective on rapid water flow in connected soil structures, Phil. Trans. R. Soc. B, 1–10, doi:10.1098/rstb.2009.0308, 2010.

HESSD
9, 10595–10655, 2012

Table 1. Laboratory measurements of average hydraulic properties for typical Weiherbach soils (after van Genuchten, 1980 and Mualem, 1976): saturated hydraulic conductivity k_s, porosity θ_s, residual water content θ_r, air entry value α, shape parameter n.

	k_s [m s^{-1}]	θ_s [m^3 m^{-3}]	θ_r [m^3 m^{-3}]	α [m^{-1}]	n [-]
Calc. Regosol	2.1×10^{-6}	0.44	0.06	0.40	2.06
Colluvisol	1.0×10^{-5}	0.40	0.04	1.90	1.25

HESSD
9, 10595–10655, 2012

Table 2. Laboratory measurements of average hydraulic properties for typical Malalcahuello soils (after van Genuchten, 1980 and Mualem, 1976). Saturated hydraulic conductivity k_s, porosity θ_s, residual water content θ_r, air entry value α, shape parameter n.

	k_s [m s^{-1}]	θ_s [m^3 m^{-3}]	θ_r [m^3 m^{-3}]	α [m^{-1}]	n [-]
Humus	2.7×10^{-3}	0.8	0.01	24	1.25
Volcanic ash horizon 1	3.5×10^{-4}	0.72	0.06	17.7	1.2
Volcanic ash horizon 2	4.0×10^{-4}	0.68	0.2	10.6	1.34
Low permeable layer	1.6×10^{-6}	0.46	0.06	22.0	3.7

HESSD
9, 10595–10655, 2012

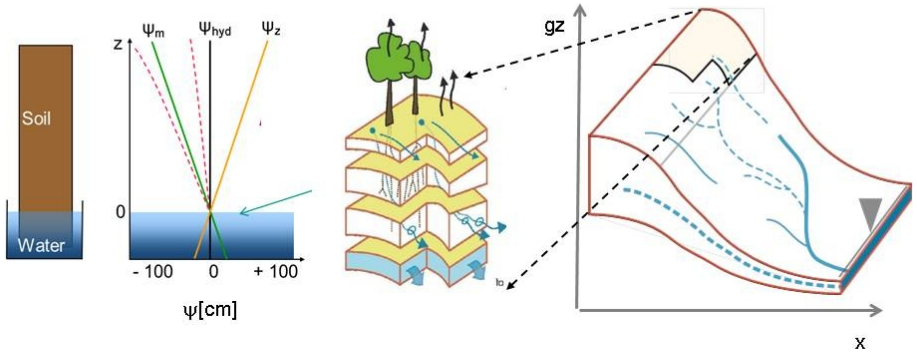

Fig. 1. Vertical and lateral flow networks and driving gradients in the critical zone at the plot and the hillslope scale. From left to right: (1) soil column with a groundwater table present; (2) equilibrium profiles of matric potential ψ_m, hydraulic potential ψ_{hyd} and gravity potential ψ_z and their disturbed shapes during radiation driven conditions; (3) diagram of the critical zone with vegetation and vertical macropores connected to lateral pipes; (4) surface and subsurface topography of a hillslope section containing a lateral pipe system with interface to the stream.

HESSD
9, 10595–10655, 2012

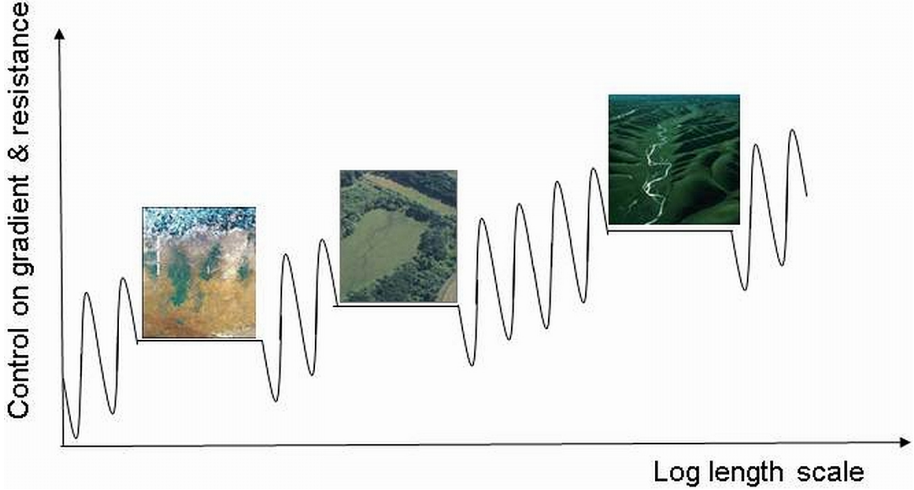

Fig. 2. Schematic hierarchy of scale levels separated by gaps of non-homogeneity with respect to controls determining either gradients or control volume resistances or boundary conditions. Possible control variables are mean and variance of soil hydraulic properties, areal density of macropores at the soil surface, areal density of pipes, rills in a lateral network.

HESSD
9, 10595–10655, 2012

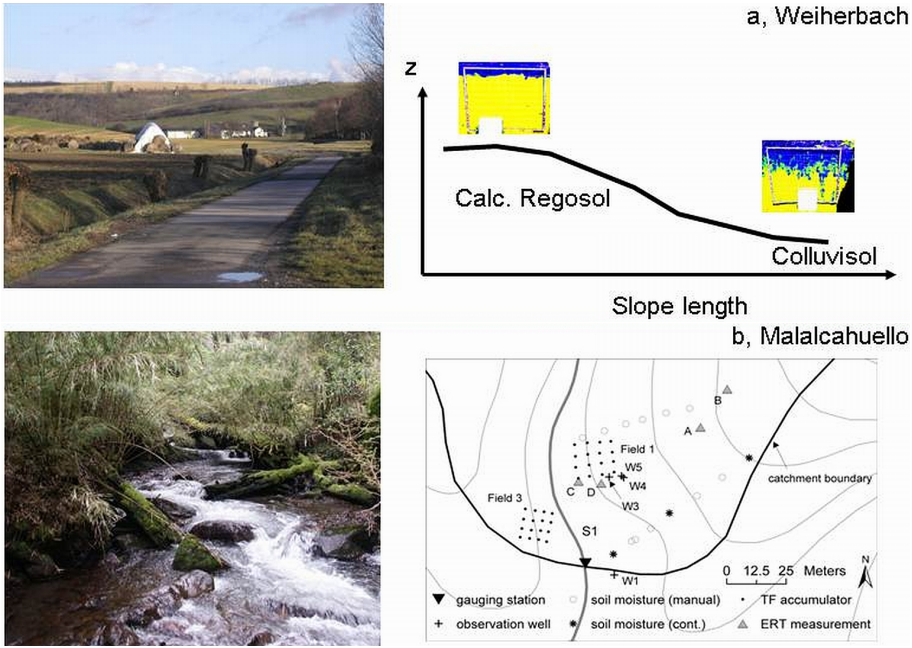

Fig. 3. (a) A typical view on the Weiherbach valley (left) and diagram of the typical spatial organization at the hillslope scale: typical catena and observed typical dye tracer patterns characterising infiltration in the different soil types. **(b)** Typical view of the Malalcahuello catchment (left) and overview of the experimental area.

HESSD
9, 10595–10655, 2012

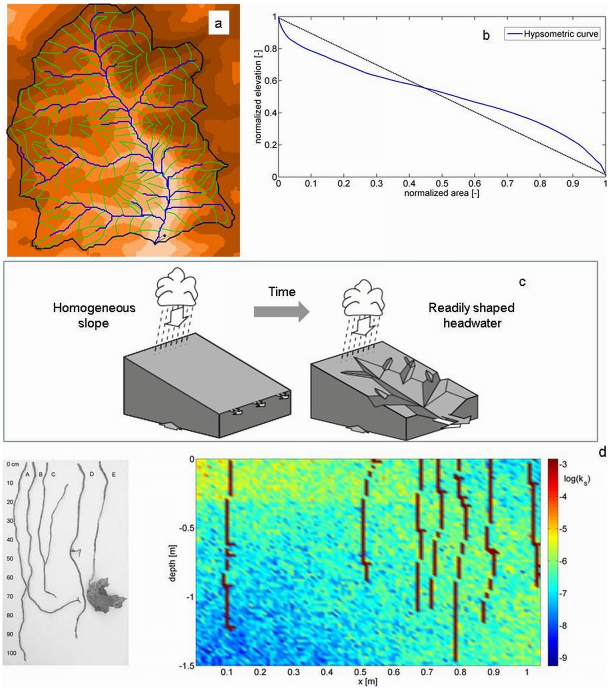

Fig. 4. (a) Digital elevation model, slope lines of steepest descent (solid green) and channel network (solid blue) that form the catchment model in case 1 of the numerical experiment 1. **(b)** The Hypsometric curve as for a mature shape of the catchment size hillslope compared to a uniform topography (the hypsometric curve is the areal fraction of pixels about a relative height h/H, where h is the height above outlet and H the total elevation difference). **(c)** Uniform configuration of a headwater according to Kleidon et al. (2012) and mature headwater with mature geomorphology with inclined valleys and a connected river net. **(d)** Structure of anecic earthworm burrows as reported in Shipitalo and Butt (1999, their Fig. 3) and (right) exemplary generation of earthworm channels of high conductivity for a 1.5 by 1 m model domain.

HESSD
9, 10595–10655, 2012

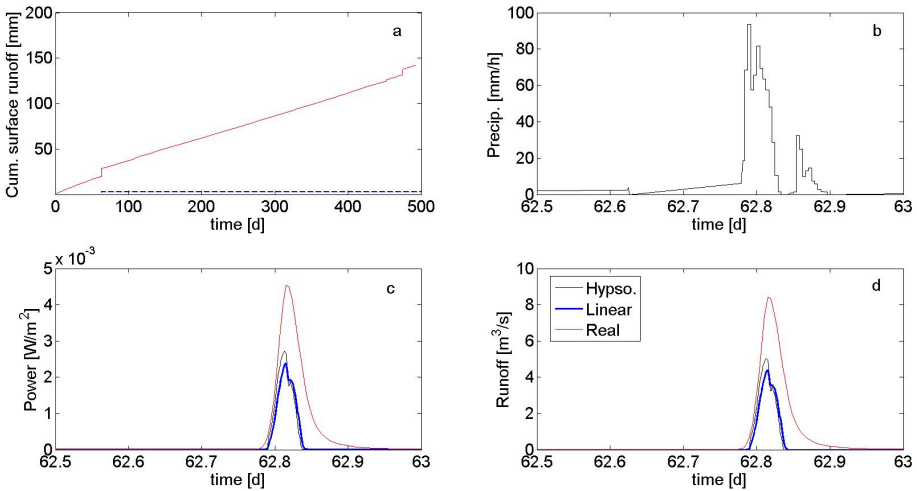

Fig. 5. Accumulated total runoff from numerical experiment 1 (Panel **a**, case 1 in solid red, case 3 in dashed blue, case 2 in solid black). Rainfall forcing at the 27 June 1994 **(b)**, simulated total runoff/surface runoff **(d)** as well as generated power for this largest observed rainfall runoff event **(c)**. Simulated runoff and generated power with the real world catchment architecture are shown in red (case 1); simulation results for the linear (case 2) and the hypsometric shaped catchment (case 3) are in blue and black, respectively. Power generation has been normalized with the surface area of the catchments.

HESSD
9, 10595–10655, 2012

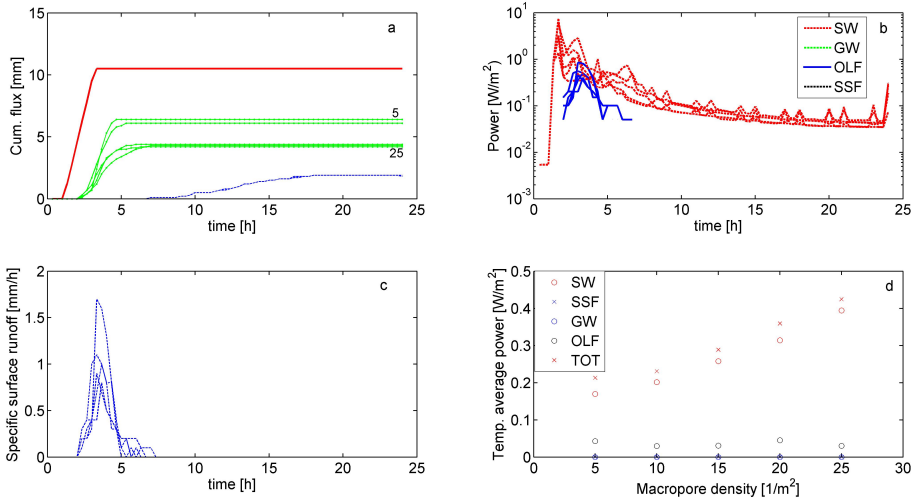

Fig. 6. Fluxes of the cumulated water balance **(a)** of the hillslope stretch: accumulated block rain (solid red), evapotranspiration (solid blue) and cumulated surface runoff in solid green. Time series of generated power **(b)** soil water flows (SW) and overland flow (OFL). Overland flow response is decreasing as expected with increasing areal density of macropores both in volume and in peak height **(c)**. Power generation averaged over one day and plotted against density of macropores **(d)**.

HESSD
9, 10595–10655, 2012

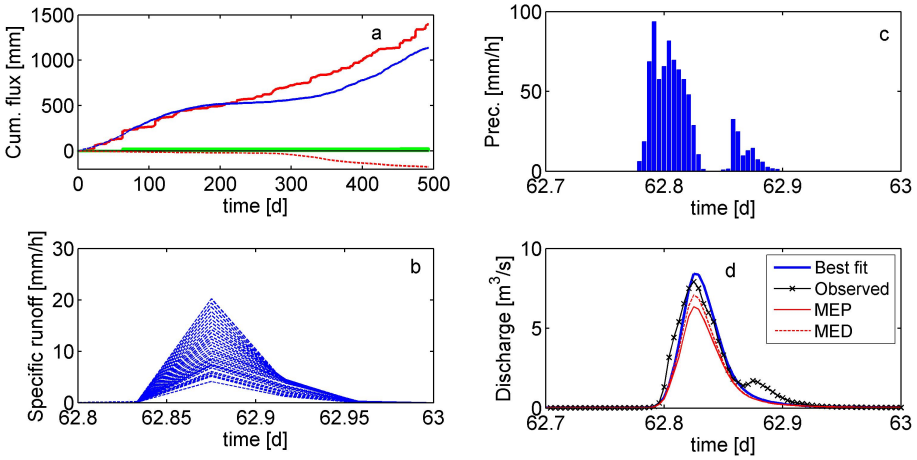

Fig. 7. (a) Accumulated fluxes of the water balance of the selected hillslope: rainfall (solid red), evapo-transpiration (solid blue), surface runoff (solid green) and groundwater recharge (dashed red, this is negative as it points downward). Note that differences for the different macroporosity values are marginal, as they only affect overland flow response during occasional events. Simulated surface runoff is strongly reduced with increasing macroporosity as shown for the largest rainfall runoff event observed in June 1994 **(b)**: note this is derived from accumulated hourly runoff). Rainfall forcing at the 27 June 1994 **(c)**. Simulated catchment scale discharge for the following model configurations **(d)** basic model setup that yielded the best fit (solid blue line), the macroporosity factor that maximized entropy production (MEP soild red line) and the macroporosity that maximized free energy reduction during the entire simulation period (MED dashed red line).

HESSD
9, 10595–10655, 2012

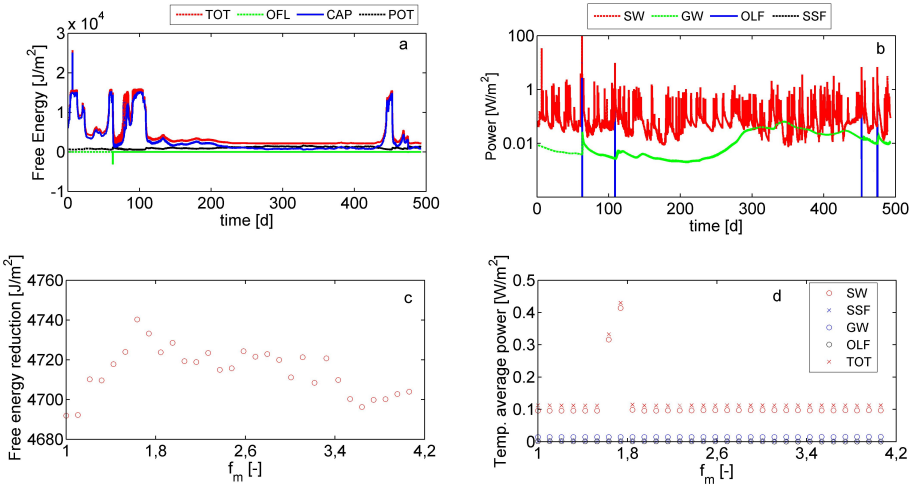

Fig. 8. Different forms of free energy plotted against time (**a**; total free energy, capillary binding energy (first term in Eq. 12), potential energy (second term in Eq. 12), kinetic energy export, (third term in Eq. 12)). Time series of power generated by different water flows (Panel **b**, soil water flow SW, groundwater recharge GW, subsurface storm flow SSF and overland flow OLF); note that, according to Eq. (4), power is equal to entropy production times the absolute temperature). Reduction of total free energy **(c)** and temporally averaged power generation for different water fluxes **(d)** plotted against the macroporosity factor f_m. Power generation and free energy have been normalized with the surface area of the selected hillslope.

HESSD
9, 10595–10655, 2012

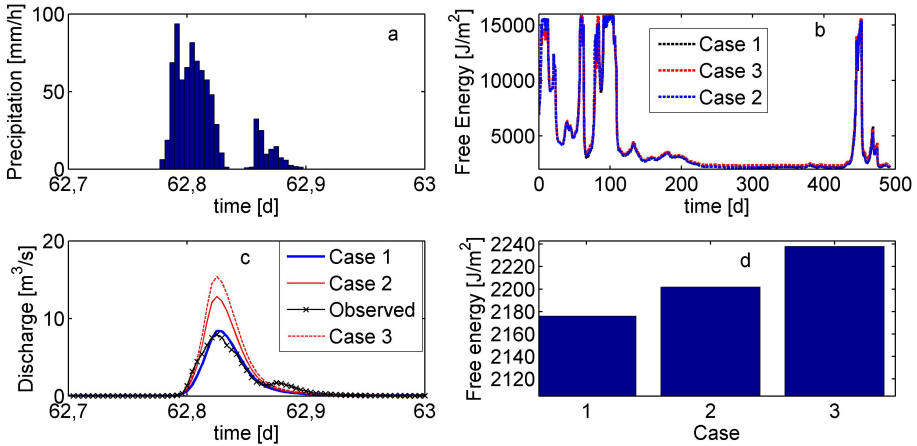

Fig. 9. Precipitation **(a)** and simulated catchment scale discharge **(c)** for Case 1 (best fit solid blue), Case 2 (flipped spatial pattern of macroporosity) and Case 3 (flipped soil and macroporosity patterns). The graphs are enlarged to the largest runoff event observed at 27 June 1994. Observed discharge is in solid black with crosses. Time series of total free energy density **(b)** as well as total free energy density at end of simulation for both cases **(d)**.

HESSD
9, 10595–10655, 2012

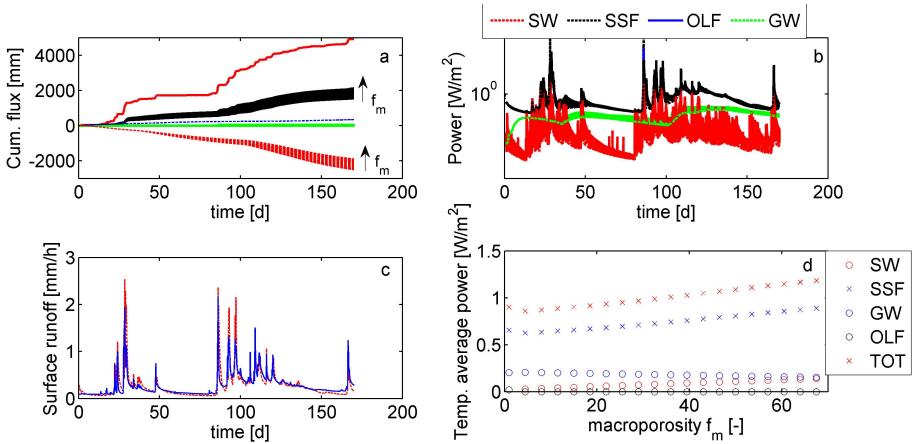

Fig. 10. Accumulated fluxes of the water balance **(a)** of the model hillslope: rainfall (solid red), evapo-transpiration (dashed blue), surface runoff (solid green), groundwater recharge (dashed red) and subsurface storm flow (solid black). For a small macroporosity the water balance is dominated by groundwater recharge, followed by subsurface storm flow; at large macroporosity values the dominance switches to subsurface storm flow. Best fit of observed specific discharge (Nash Sutcliffe efficiency 0.7) was achieved with a macroporosity of 54 (Panel **c**, observed runoff is in solid blue). Time series of power generated by different flows (Panel **b**, soil water flows SW, groundwater recharge GW, subsurface storm flow SS and overland flow OLF) and temporally averaged power generation for different water fluxes plotted against model parameter f_m. Power generation has been normalized with the surface area of the hillslope.

HESSD
9, 10595–10655, 2012